DETERMINATION OF AN ANALYTICAL RELATIONSHIP BETWEEN ENTROPY GENERATION AND MIXING EFFICIENCY FOR MICROMIXER APPLICATIONS

A Thesis Presented

By

Aric Martin Gillispie

Presented to the Jackson College of Graduate Studies of the University of Central Oklahoma in Partial Fulfillment of the Requirements for the Degree of

MASTER OF SCIENCE IN ENGINEERING PHYSICS – MECHANICAL ENGINEERING

May 2017

This thesis is approved for recommendation to the

University of Central Oklahoma Jackson College of Graduate Studies

DETERMINATION OF AN ANALYTICAL RELATIONSHIP BETWEEN ENTROPY GENERATION AND MIXING EFFICIENCY FOR MICROMIXER APPLICATIONS

By

Aric M. Gillispie

Thesis Committee Chair:

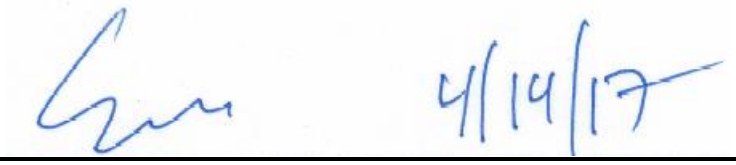

Dr. Evan Lemley

Thesis Committee Members:

Dr. Mohammed Hossan

Dr. Abdellah Ait Moussa

ABSTRACT

DETERMINATION OF AN ANALYTICAL RELATIONSHIP BETWEEN ENTROPY GENERATION AND MIXING EFFICIENCY FOR MICROMIXER APPLICATIONS

May 2017

Aric Martin Gillispie

University of Central Oklahoma

Directed by: Dr. Evan Lemley

Abstract

This thesis presents a detailed computational analysis for a simple tee micro-mixing geometry. Micromixers have broad applications in heat exchangers and lab-on-chip (LOC) devices. Simply, a micromixer seeks to efficiently and quickly exchange one or more physical quantities, such as temperature or molecular concentration. The measure of how completely these quantities are exchanged is known as the mixing efficiency. For LOC devices an effective design will be simple and cost effective to manufacture, and provide the greatest mixing efficiency for the smallest device as rapidly as possible.

The work here has two main objectives. First, an analytical relationship is sought that functionally relates the entropy generation to the mixing index for a simple tee shaped micromixer. Second, the work will serve as a guide to improve an existing micromixer through its developed methods. A thorough computational fluid dynamics (CFD) analysis is performed for a wide range of Reynolds numbers typical to micromixers with varying flow parameters. The result are several analytical relationships that relate the relevant quantities of entropy generation

rate and mixing efficiency to the known flow and fluid parameters. Additionally, a simple relationship is derived that relates the mixing efficiency directly to the entropy generation rate effectively proving a direct relationship between the two quantities. Finally, the relevant results are used to propose a design for a micromixer that provides high mixing efficiencies for a wide range of operating conditions.

Acknowledgements

This work was made possible by the Department of Engineering and Physics at the University of Central Oklahoma, under the supervision of Assistant Dean, Professor and Faculty Mentor Dr. Evan Lemley. I would like to express gratitude to Dr. Evan Lemley for his five years of mentoring through my undergraduate and graduate research endeavors. Additionally, much of this work builds upon research that was made possible by four Research, Creative, and Scholarly Activities grants awarded by the Office of Research and Grants at the University of Central Oklahoma. Finally, this work was partially sponsored by the National Science Foundation grant ACI-1429702 (funding for the Buddy Supercomputer Cluster), which served as the platform for much of the analyses conducted for this thesis. I would like to thank Ivan Gutierrez a part of the University of Central Oklahoma College of Math and Science technology team for his help in ensuring that the computational demands required by this thesis were met as effectively as possible.

Contents

List of Tables and Figures

Nomenclature

Symbols	
L	A quantity / Length of a Branch
V	Volume
t	Time
A	Area
$\mathbf{v}$	Velocity
$\mathbf{n}$	Unit normal vector
Q	Volume flow rate
F	Force
$\frac{\mathrm{D}}{\mathrm{Dt}}$	Total Derivative
MI	Mixing Index
w_f	Flow Weight
$\dot{s}$	Entropy generation rate
C	Concentration /Cross Sectional Slice
C_o	$(C_1 - C_2)/2$
T	Temperature
R	Ideal gas constant
D	Molecular Diffusivity
K	Thermal Conductivity
u	x-direction velocity
v	y-direction velocity
w	z-direction velocity
U	non-dimensional x-direction velocity
W	non-dimensional y-direction velocity
Z	non-dimensional z-direction velocity
D_h	Hydraulic Diameter
Re	Reynolds Number
$f(\ \ )$	Function of ()
P	Pressure/ Normalizing Function
G	Gap Ratio
W	Width
H	Gap Thickness
W_b	Gap Width

Greek Symbols	
∇	Gradient
$\partial/\partial t$	Partial Derivative
ρ	Density
σ	Stress Tensor/ Standard Deviation
∇^2	Laplacian
μ	Viscosity
Δ	Difference
γ	Irreversibility Distribution Ratio
α, ω, ξ	Constants to be Determined

Superscripts	
∇	Gradient
Subscripts	
b	Body
0	Initial
o	Out
F	Friction part
T	Temperature part
D	Concentration Diffusion Part
in	Inlet
nd	Non-Dimensionalized
i	Variable/inlet number

Chapter I: Literature Review

I.1 Introduction

Micromixers and microfluidic devices are making great strides in offering affordable and portable alternative solutions to large scale devices. Microfluidic devices provide a platform for biomedical applications such as medical delivery and tests and mechanical applications such as heat-exchangers, and a wide range of chemical applications [1-2]. Often times, these devices' functionality rely heavily on mixing. As such, many of these devices are termed micromixers. In the development of micromixers, the goal is to achieve the greatest mixing efficiency with the lowest energy expenditure, at the smallest possible size. This has led to many creative and innovative micromixer designs [3-14]. However, each of these share one main commonality. Each device serves to transport a quantity from one fluid to another, even if the fluid differs by something as simple as the temperature.

I.2 Active Micromixers

Micromixers are classified into two categories: active and passive. Active micromixers utilize some mechanical means of physically causing the fluids to interact in a productive way[21]. The most common types of active micromixers include acoustic, dielectrophoretic, electrokinetic time-pulsed, electrodynamic force, thermal actuation, magneto-hydrodynamic flow, and electrokinetic instability. Regardless of the type, each requires some form of external power. As a result, the high mixing efficiencies is often overshadowed by the complexity and the cost of manufacturing of the device. *Table 1* outlines the types of active micromixers.

Acoustic micromixers, or surface acoustic wave (SAW) micromixers, are active micromixers that use sound waves to enhance mixing in laminar flows. This is accomplished

through the use of electrodes that apply alternating current (AC) voltages at specific frequencies that can generate waves on the fluid surface[1]. A major benefit to this type of active micromixers is its relative simplicity and large mixing forces.

In a similar fashion, dielectrophoretic micromixers utilize AC or DC voltages to produce electro-osmotic flows through the use of low voltage generated electrokinetic rolls using microparticles [15]. Unlike acoustically disturbed flows, electrokinetic flows seek to make use of the electric field lines to stir the flow in the plane normal to the flow. Likewise, electrokinectic time pulsed mixers drive the fluid through the use of conductive particles, and mix them through pulsing the voltages [16].Further utilizing the conductive properties of various fluids (specifically fluids with identical viscous and inertial properties), the electrohyrdrodynamic [17] and magneto –hydrodynamic [18] mixing techniques enhance mixing in traditional laminar micromixers.

Finally, among the common active micromixers are those that utilize pressure and thermal perturbations. In pressure perturbation micromixers, the pressure is pulsed, generating rapid changes in downstream fluid velocities causing increased fluid species interaction[19]. Conversely, thermal actuation can be used to introduce bubbles into the microchannels that act as the mixing mechanism[20]. The mixing lengths, and achieved mixing indices are outlined in *Table 1.*

Table 1: Summary of Active Micromixers

Category	Mixing Length (D_h)	MI	Reference
Dielectrophoretic	12.5	0.85	[15]
Magneto Hydrodynamic Flow	5	0.977	[18]
Acoustic	112.5	0.9	[23]
Electrokinetic Time Pulsed	2.5	0.88	[24]
Electrokinetic Instability	4.6	0.98	[26]

I.3 Passive Micromixers

The alternative to active mixers are passive micromixers. Passive micromixers fall within a wide variety of categories, and often rely on a combination of multiple types of mixing. Specifically, passive micromixers rely solely on the micromixing geometry to increase contact area between the fluids, with a dominating mixing medium of diffusion.

To this end, to increase mixing in passive micromixers, there currently exist two modes of mixing: chaotic advection and diffusion. Chaotic advection occurs when the geometry is designed to fold the fluids into each other to force interaction. Diffusion on the other hand is a function of time and contact area; therefore, mixing is often increased through lamination or injection. Naturally, quantities move from higher concentration to lower concentration and, when given enough time and contact area, will reach some maximum value of mixing.

I.3.1 Chaotic Advection

Chaotic advection is a form of mass transfer that is utilized to increase the mixing efficiencies of micromixers. In general, chaotic advection occurs in directions perpendicular to the flow direction, increasing contact area and forcing the different fluid species to interact in a

productive way. This is mostly accomplished through a specific channel geometry that causes the fluid to split and recombine, fold, stretch, or break. Common flow geometries are implemented for a variety of different flow cases. These flow geometries include obstacles placed in the mixing length of the body[4][14], complicated two-dimensional and three-dimensional channels such as the 2D tesla [5], or variations of a 3D serpentine [27-31]. However, these geometries require special and complex manufacturing techniques that increase the cost of implementing them in common applications. A common improvement over the three-dimensional micromixers, are two-dimensional geometries that incorporate a patterned wall with ribs and grooves at various angles in a variety of configurations[33-37]. *Table 2* outlines the types of chaotic advection based mixers, and the typical flow parameters.

Table 2: Passive Chaotic Advection Micromixers

Disturbance	Typical Velocities (mm/s)	Typical Reynolds Number	Reference
Zig-Zag	1.3-40	0.26-267	[14]
3D Serpentine	1-2000	0.1-70	[27-31]
Source-Sink	-------	-------	[32]
Cylindrical Obstacles	0.17-20	0.2-0.25	[38][39]
Patterned Wall	0.01-50	0.01-6.65	[33-37]
2D Tesla	5	6.2	[40]

I.3.2 Diffusion

The other form of mixing specifically utilizes the natural tendency of species to migrate from areas of high to low concentration through fluid contact, or diffusion. As such, the most productive means of increasing diffusion is causing the flow to increase its contact area. There are two mechanisms for accomplishing this task: lamination and injection. Lamination is the process of splitting the flow into sub-streams and then recombining them inside the opposite

fluid species. This effectively increases the fluid contact area from one face of contact to several. Parallel lamination occurs when the flow is laminated in a single direction, where serial lamination constantly laminates the flow in and out of planar directions (stages) using three-dimensional channels. Injection simply forces the fluids of a one fluid species perpendicularly into the sides of the other fluid. *Table 3* outlines typical parameters for diffusion micromixers.

Table 3: Diffusion Passive Micromixers

Parallel Lamination	Type	Typical Velocities (mm/s)	Typical Reynolds Number	Reference
	"T"	0.17-7000	0.3-500	[43-48]
	"Y"	0.27-200	0.4-80	[49-52]
	Vortex	10000	200	[53]
	Cross Shaped	5000-10000	170-340	[54]
	Parallel	0.7-1.5	0.0035-0.07	[55] [56]
	Focusing	1-50	0.15-0.5	[57] [58]
Serial Lamination Micromixers	Number of Stages	Typical Velocities	Typical Reynolds Number	Reference
	3	1-22	0.03-0.66	[59]
	5-20	1.8	0.072	[60]
	6	0.5	0.05	[61] [62]
	1	0.25	0.0025	[63]
	16	2	0.1	[64]
Injection Micromixers	Number of Nozzles	Typical Velocities	Typical Reynolds Number	Reference
	400	1.2	0.018	[65][66]
	10-20	1	0.1	[67]
	1	15	0.1	[68] [69]

I.3.3 Summary

Balancing chaotic advection and diffusion must lead to a passive micromixer that will yield an acceptable mixing efficiency in a desirable size and reasonable time. Typical mixing lengths and corresponding mixing efficiencies can be found in *Table 4.*

Table 4: Summary of Passive Micromixers

Category	Type	Mixing Length (D_h)	MI	Reference
Lamination	Wedge Shaped Inlets	0.0667	0.9	[71]
Zig-Zag	Elliptic-shape Barriers	164	0.96	[72]
Embedded Barriers	Vortices	64	0.72	[73]
Twisted Channels	SAR	36	1	[74]
Surface	Obstacle Shape	10	0.98	[75]
Surface	T/Y mixer	10	0.95	[76]

I.4 Background

There are two quantities that are important when considering micromixers. Micromixers show a heavy reliance on the Reynolds numbers being achieved within the device. The Reynolds number is a dimensionless quantity that provides the ratio of inertial forces to viscous forces within a fluid species at a certain flow rate. Entropy generation is a quantity that defines the irreversibility of a system, and is often useful when discussing micromixers. Entropy generation can be determined for any quantity within a system. The available literature is replete with discussions on entropy generation in different applications [91-100]. There are much fewer sources that discuss a possible relationship between entropy generation and mixing efficiency [9] that ultimately yield no analytical relationship. In fact, the relationships found in Muradoglu et al [9] are the closest results that can be found that could lend themselves to a direct means of determining an analytical relationship, though this is neither recognized nor pursued in [9], and the type of mixer and even the analysis are vastly different than the results presented in this thesis.

I.5 Thesis Statement and Objectives

This thesis seeks to determine an analytical relationship among relevant quantities in the simplest form of a micromixer, a tee junction. A tee combines two fluids at anti-parallel branches, thus making it possible for the fluids to interact through parallel lamination. For this geometry, a working relationship between the Reynolds numbers of the fluids, the entropy generation rate, and the mixing efficiency will be sought. Additionally, these relationships will be pursued in such a way that they are independent of scale or include a simple conversion for any arbitrary scale. This is important because it provides the possibility of validation regardless of the experimental size constraints. Using the work from the thesis, the goal is to improve existing micromixers (either in size reduction, time decrease, or mixing efficiency increase) by the use of a tee junction to combine two fluids. A macro-scale (order of centimeters) and micro-scale geometry is created, and ANSYS Fluent simulations are conducted to calculate the volumetric entropy generation rates and the concentration fields in a three-dimensional model. This analysis is conducted over a range of Reynolds commonly accepted to occur in microchannels (0-200), with varying flow weightings at the inlets to increase parallel lamination and induce chaotic advection in the absence of flow obstacles. Finally, the work of the thesis is applied in improving a micromixer that incorporates two modes of passive mixing: injection and chaotic advection, through the design of simpler mixer that utilizes chaotic advection and lamination. The summary of the objectives is provided below.

1. Determine a relationship between the mixing efficiency and the Reynolds number for several simple tee micromixers.
2. Determine a relationship between the volumetric entropy generation rate and the Reynolds number for several simple tee micromixers.

3. Determine a relationship between the mixing efficiency and the volumetric entropy generation rate for several simple tee micromixers.
4. Develop relationships that hold for any scale.
5. Develop a simple micromixer that is an improvement on a current high efficiency micromixer.

Chapter II: Theory

II.1 Governing Equations

The general form for conservation of a quantity L is derived from the fact that the sum of all changes in a control volume V must be equal to the sum of the losses and gains in that system. In integral form this is presented by:

$$\frac{d}{dt}\int_V L\, dV = -\int_{C.S.} L\, \mathbf{v}\cdot\boldsymbol{n}\, dA - \int_{C.V.} S\, dV \qquad 1$$

Where $\mathbf{v}$ is the velocity across the surface, $\mathbf{n}$ is the unit vector normal to the surface, and S represents the sources and sinks within the system. Applying this general form to momentum and mass respectively leads to:

$$\rho\left(\frac{\partial \mathbf{v}}{\partial t} + \mathbf{v}\cdot\nabla\mathbf{v}\right) = \boldsymbol{F_b} \qquad \text{Conservation of Momentum}$$

Where:

$$\frac{\partial \mathbf{v}}{\partial t} + \mathbf{v}\cdot\nabla\mathbf{v} \equiv \frac{\mathrm{D}\mathbf{v}}{\mathrm{D}t} \qquad \text{Material Derivative of } \mathbf{v}$$

And

$$\frac{\partial \rho}{\partial t} + \nabla\cdot(\rho\mathbf{v}) = 0 \qquad \text{Conservation of Mass}$$

Where F_b is a general body force. The body force can be described more specifically for a real case by defining the body force to be a sum of the forces resulting from stresses on the control volume and the external forces to the system. Specifically,

$$F_b = \nabla \cdot \sigma + F \qquad 2$$

Where σ is the stress tensor, and F is the sum of external forces. Separating the stress tensor into normal and shear stresses leads to the simplification of the *Conservation of Momentum* equation. The simplification comes from defining:

$$\sigma_{ij} = \begin{pmatrix} \sigma_{11} & \tau_{12} & \tau_{13} \\ \tau_{21} & \sigma_{22} & \tau_{23} \\ \tau_{31} & \tau_{32} & \sigma_{33} \end{pmatrix} = -(P)\begin{pmatrix} 1 & 0 & 0 \\ 0 & 1 & 0 \\ 0 & 0 & 1 \end{pmatrix} + \begin{pmatrix} \sigma_{11} + P & \tau_{12} & \tau_{13} \\ \tau_{21} & \sigma_{22} + P & \tau_{23} \\ \tau_{31} & \tau_{32} & \sigma_{33} + P \end{pmatrix}$$

Where one can define:

$$\begin{pmatrix} \sigma_{11} + P & \tau_{12} & \tau_{13} \\ \tau_{21} & \sigma_{22} + P & \tau_{23} \\ \tau_{31} & \tau_{32} & \sigma_{33} + P \end{pmatrix} = \boldsymbol{\sigma'} \qquad 3$$

Therefore,

$$\rho \frac{D\boldsymbol{v}}{Dt} = -\nabla P + \nabla \cdot \boldsymbol{\sigma'} + F \qquad 4$$

Applying the following assumptions appropriate for an incompressible, Newtonian fluid, with constant viscosity, the above equations reduce to the Navier-Stokes equations:

$$\rho \frac{\partial \boldsymbol{v}}{\partial t} + \rho \mathbf{v} \cdot \boldsymbol{\nabla} \mathbf{v} = -\boldsymbol{\nabla} P + \mu \boldsymbol{\nabla^2} \mathbf{v} + \mathrm{F}$$

Where μ is the viscosity of the fluid. Applying a similar analysis for the species concentration of a fluid leads to:

$$\frac{\partial C}{\partial t} + \mathbf{v} \cdot \nabla C = D\nabla^2 C \tag{5}$$

Where C is the local concentration and D is the diffusivity of the fluid assumed here to be a constant. These equations when discretized to a finite volume provide the means by which a solution can be determined computationally using the finite volume method.

For the analysis conducted by this thesis, a method for calculating the mixing efficiency and the volumetric entropy rate is necessary. First, considering the mixing efficiency, Hossain, et al. [3] provides a method for determining the mixing index MI as a function of the distributions of mass fractions in plane of a system such that:

$$MI = 1 - \sqrt{\frac{\sigma^2}{\sigma_{max}^2}} \tag{6}$$

Where σ^2 is the variance of the mass fraction and $\sigma_{\max}^2$ is the maximum variance that would occur for plane divided by weighted flow area, if no mixing would occur. Therefore

$$\sigma^2 = \sqrt{\frac{1}{N}\sum_{i=1}^{N}(C_i - \bar{C})^2} \tag{7}$$

Where C_i is the local concentration at a cell numbered i and $\bar{C}$ is the average concentration of the plane. To determine $\sigma_{\max}^2$ one should consider the weighted flow area plots. Considering two species with mass fractions *1* and *0* respectively with a flow weighting of:

$$w_f = \frac{Q_2}{Q_1} \qquad where\ Q_2 > Q_1 \tag{8}$$

and Q is the volume flow rate at the inlets, with inlet *1* having a mass fraction of *0* and inlet *2* having a mass fraction of *1*. The area weighted plots for unmixed flow with flow weighting w_f is shown in *Figure 1*.

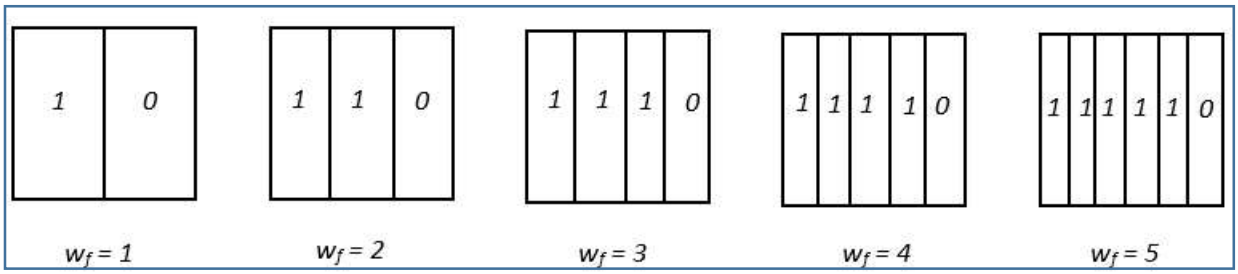

Figure 1: Graphical Determination of w_f

Where σ_{max}^2 is presented in *Table 5*.

Table 5: Flow Weighting and Maximum Variance

w_f	1	2	3	4	5
σ_{max}^2	0.25	0.44	0.56	0.64	0.69

From the above, *MI* can be calculated, and the mixing efficiency can be determined to be α where:

$$\alpha = MI * 100 \tag{9}$$

Examining the volumetric entropy generation rate, it is often considered to be the sum of thermal and viscous entropy terms. In Cartesian coordinates the volumetric entropy generation rate is:

$$\dot{s}''' = \frac{\mu}{T_o}\left[2\left(\left(\frac{\partial u}{\partial x}\right)^2 + \left(\frac{\partial v}{\partial y}\right)^2 + \left(\frac{\partial w}{\partial z}\right)^2\right) + \left(\frac{\partial u}{\partial y} + \frac{\partial v}{\partial x}\right)^2 + \left(\frac{\partial u}{\partial z} + \frac{\partial w}{\partial x}\right)^2 + \left(\frac{\partial v}{\partial z} + \frac{\partial w}{\partial y}\right)^2\right] + \frac{K}{T_o^2}\left[\left(\frac{\partial T}{\partial x}\right)^2 + \left(\frac{\partial T}{\partial x}\right)^2 + \left(\frac{\partial T}{\partial x}\right)^2\right] \tag{10}$$

Where the viscous contribution is:

$$\dot{s}_F{}''' = \frac{\mu}{T_o}\left[2\left(\left(\frac{\partial u}{\partial x}\right)^2 + \left(\frac{\partial v}{\partial y}\right)^2 + \left(\frac{\partial w}{\partial z}\right)^2\right) + \left(\frac{\partial u}{\partial y} + \frac{\partial v}{\partial x}\right)^2 + \left(\frac{\partial u}{\partial z} + \frac{\partial w}{\partial x}\right)^2 + \left(\frac{\partial v}{\partial z} + \frac{\partial w}{\partial y}\right)^2\right] \quad 11$$

And the thermal contribution is:

$$\dot{s}_T{}''' = \frac{K}{T_o^2}\left[\left(\frac{\partial T}{\partial x}\right)^2 + \left(\frac{\partial T}{\partial x}\right)^2 + \left(\frac{\partial T}{\partial x}\right)^2\right] \quad 12$$

Expanding this term to include the volumetric entropy rate associated with concentration gradients (both space and temperature affected) leads to:

$$\dot{s}''' = \dot{s}_F{}''' + \dot{s}_T{}''' + \frac{RD}{C_o}\left[\left(\frac{\partial C}{\partial x}\right)^2 + \left(\frac{\partial C}{\partial y}\right)^2 + \left(\frac{\partial C}{\partial z}\right)^2\right] + \frac{RD}{T_o}\left[\left(\frac{\partial T}{\partial x}\right)\left(\frac{\partial C}{\partial x}\right) + \left(\frac{\partial T}{\partial y}\right)\left(\frac{\partial C}{\partial y}\right) + \left(\frac{\partial T}{\partial z}\right)\left(\frac{\partial C}{\partial z}\right)\right] \quad 13$$

However, this thesis explores the isothermal case such that:

$$\dot{s}''' = \dot{s}_F{}''' + \dot{s}_D{}''' \quad 14$$

Where

$$\dot{s}_D{}''' = \frac{RD}{C_o}\left[\left(\frac{\partial C}{\partial x}\right)^2 + \left(\frac{\partial C}{\partial y}\right)^2 + \left(\frac{\partial C}{\partial z}\right)^2\right] \quad 15$$

To be of the most convenient form, a non-dimensionalized version of the above equation will be sought, consistent with the non-dimensionality of the mixing index and the Reynolds number. The following non-dimensionalized terms are introduced:

$$U = \frac{u\rho D_h}{Re_o\mu}, \quad V = \frac{v\rho D_h}{Re_o\mu}, \quad W = \frac{w\rho D_h}{Re_o\mu}, \quad X = \frac{x}{D_h}, \quad Y = \frac{y}{D_h}, \quad Z = \frac{z}{D_h}, \quad \Phi = \frac{C - C_o}{\Delta C} \quad 16$$

And

$$Re_{out} = \frac{\bar{v}\rho D_h}{\mu} \quad 17$$

Non-dimensionalizing using these factors leads to:

$$\dot{s}_{nd}''' = \gamma_1 \dot{s}_{F,nd}''' + \gamma_2 \dot{s}_{D,nd}''' \quad (18)$$

Where:

$$\dot{s}_{nd}''' = \frac{\dot{s}''' T_o \rho^2 D_h^2}{\mu^3} \quad (19)$$

$$\dot{s}_{F,nd}''' = \left[2\left(\left(\frac{\partial U}{\partial X}\right)^2 + \left(\frac{\partial V}{\partial Y}\right)^2 + \left(\frac{\partial W}{\partial Z}\right)^2\right) + \left(\frac{\partial U}{\partial Y} + \frac{\partial v}{\partial X}\right)^2 + \left(\frac{\partial U}{\partial Z} + \frac{\partial W}{\partial X}\right)^2 + \left(\frac{\partial V}{\partial Z} + \frac{\partial W}{\partial Y}\right)^2\right] \quad (20)$$

$$\dot{s}_{D,nd}''' = \left[\left(\frac{\partial \Phi}{\partial X}\right)^2 + \left(\frac{\partial \Phi}{\partial Y}\right)^2 + \left(\frac{\partial \Phi}{\partial Z}\right)^2\right] \quad (21)$$

$$\gamma_1 = Re_{out}^2 \quad (22)$$

$$\gamma_2 = \frac{2RDT_o \rho^2 D_h^2 \Delta C}{\mu^3} \quad (23)$$

With γ being a non-dimensionalized weighting factor.

II.2 Solution Models

To conduct the computational analysis, *ANSYS® Fluent®* was used. A pressure based solver was employed to obtain steady state solution for laminar flow while obtaining solutions for the energy equation and species transport. To obtain a solution, the volume was discretized by interpolating the field variables located at the cell centers to the connecting faces of each control volume. The solution was obtained for pressure-velocity coupling using the semi-implicit method for pressure-linked equations (SIMPLE). The pressure, momentum, species concentration, and energy were all discretized using a Second Order Upwind scheme, for increased accuracy over the range of conducted flows. The gradients were determined using the least-squares cell based method, essentially a node-based solution method. After discretization,

Fluent® solves and bases convergence on the continuity equations, energy equations, and concentration gradients where the residuals for convergence are held at 10^{-6}.

II.3 Form of Results

In order to satisfy the thesis objectives, simulations were conducted to determine analytical relationships between the relevant design quantities: Reynolds number, mixing efficiency, and volumetric entropy generation rate. For a tee with combining fluids in the anti-parallel branches, a non-dimensionalized linear relationship is sought to satisfy the following forms:

$$f(\dot{s}) = f(Re) + \alpha \tag{24}$$

$$f(MI) = f(Re) + \alpha \tag{25}$$

Where *Equation 25* and *26* can be used to develop an analytical relationship for the entropy generation rate and the mixing index where:

$$f(\dot{s}) = f(MI) + \alpha \tag{26}$$

With α being a constant to be determined. The analytical expression should be non-dimensionalized and independent of scale. Using this approach one could determine similar relationships for more complex geometries or estimate the effect of the easily determined fluid parameters in the development of similar micromixers. This thesis will use the determined relationships to improve existing micromixers through size reduction, shortening of mixing time, and increased mixing efficiency for existing or new micromixers.

Chapter III: Methodology

III.1 Preprocessing

The information that *Fluent*® requires is the inlet velocities (such that the desired Reynolds number is satisfied) where:

$$v_{in} = \frac{\mu Re_{in}}{D_h \boldsymbol{\rho}} \tag{27}$$

The pressure is not specified which allows *Fluent*® to calculate the necessary pressures that are required to achieve the specified flow rates. Finally, the diffusivity of the fluid species should be specified. The diffusivity of fluid *A* inside another fluid species *B* is defined by the Wilke-Change correlation [103]:

$$D_{AB} = \frac{7.4 * 10^{-8} (\boldsymbol{\Phi} M_B)^{0.5} T}{\mu_D v_B^{0.6}} \tag{28}$$

III.2 Model Formulation

The model that is used for the analysis is a simple *tee* micromixer, where the fluid enters at anti-parallel branches and exits at the remaining and outgoing branch (*Figure 2*). The anti-parallel branches of the tee have lengths consistent with the study that will be performed and the outgoing branch is long enough to be able to assume that the fluid is fully developed at the exit. This is known as outflow. There are two factors that are explored independently: flow weight at the inlets, and the amount that the fluid is developed at the inlets. To account for the latter, the model is designed to have inlet branches that are sufficiently long as determined by

$$\frac{L_e}{D_h} = 0.06Re \tag{29}$$

To allow for consistent and accurate results, the inlet branches are determined by the maximum Reynolds number that will be explored. In the case of exploring flow that is not fully developed. Branch inlets are taken to be long enough to specify a distance beyond the tee junction, but short enough to allow the fluid to be developed to differing degrees. The tee junction itself is defined by:

$$L1 = L2 = L3 = 0.5D_h$$

However, the following lengths are considered to generate the models used for analysis.

Table 6: Naming Convention for Thesis Models

L1 (D_h)	**L2 (D_h)**	**Fluid Result at Junction**	**Model Name**
35.5	35.5	Both Fully Developed	L
35.5	2	One Side is fully developed, the other Developing	H
2	2	Both Developing	S

The assumptions made for the computational analysis of flow are: steady state, pressure driven, and fully developed at the outlet. The flow is Newtonian and laminar, satisfying the reduced form of the Navier-Stokes equations (*Equation 5*). Additionally, the flow is isothermal with boundaries that are assumed to be non-slip and insulated. From these assumptions, *Fluent*® can derive the results for the velocities, pressures, concentrations, and related gradients for which the analysis will be conducted.

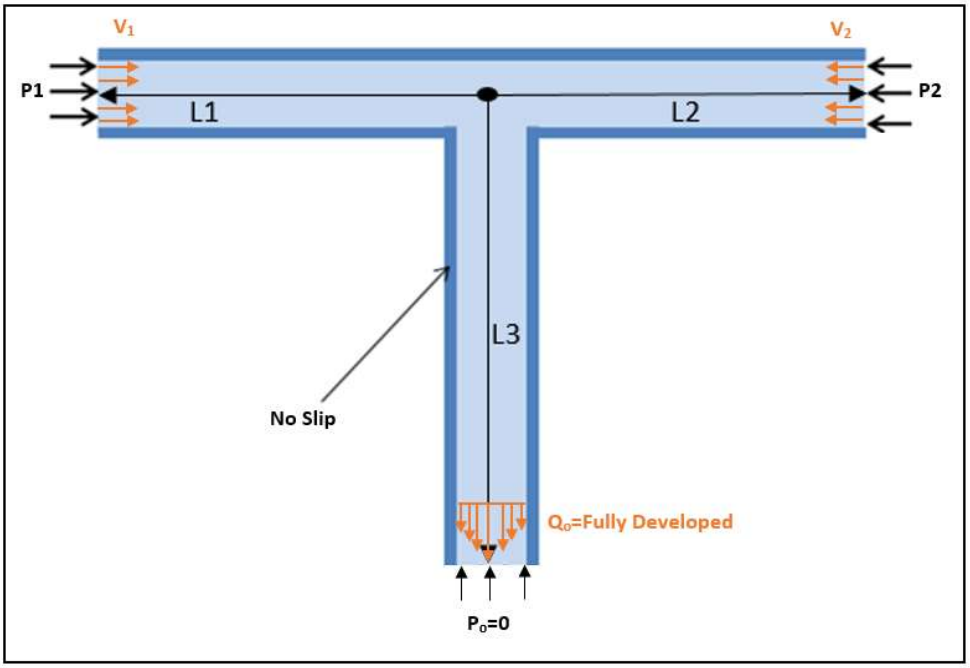

Figure 2: Thesis Model

The hydraulic diameter is defined as:

$$D_h = \frac{4 * Area}{Perimeter} \tag{30}$$

However, when considering a rectangular geometry defined as in *Figure 3.*

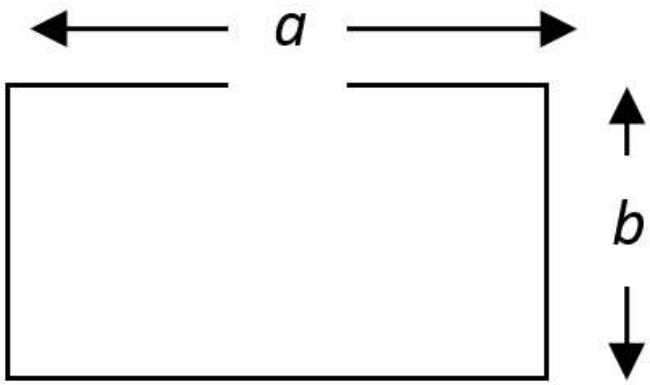

Figure 3: Aspect Ratio of a Rectangular Geometry

Equation 31 simplifies to:

$$D_h = \frac{4ab}{2(a+b)} \quad 31$$

The relationship for a and b is defined by:

$$R = \frac{a}{b} \quad 32$$

For much of the thesis a square duct is considered or more specifically a duct with

$$R = 1 \quad 33$$

In the consideration of different flow weights (w_f), input parameters would be modified to satisfy *Equation 9*. *Table 7* shows the convention for the model naming suffixes.

Table 7: Model Suffixes

w_f	Model Suffix
1	W1
2	W2
3	W3

Similarly, higher values of w_f will yield corresponding suffixes. Due to the asymmetry of model *H*, it is important to note that when considering different flow weights, either branch could contain the faster moving fluid. To account for this, model *H* must be further classified to describe the status of the flow in each branch.

Table 8: Further Naming Convention of the H Model

Flow Description	Model Prefix
The flow is faster in the longer branch	H*l*
The flow is faster in the shorter branch	H*s*

The analysis is further conducted to explore the impact of Reynolds number on the flow, a model is created such that the inlets have differing hydraulic diameters. This can allow for the identification of the impact of Reynolds number compared to the flow rate on the model. The model that is used is shown *Figure 4.*

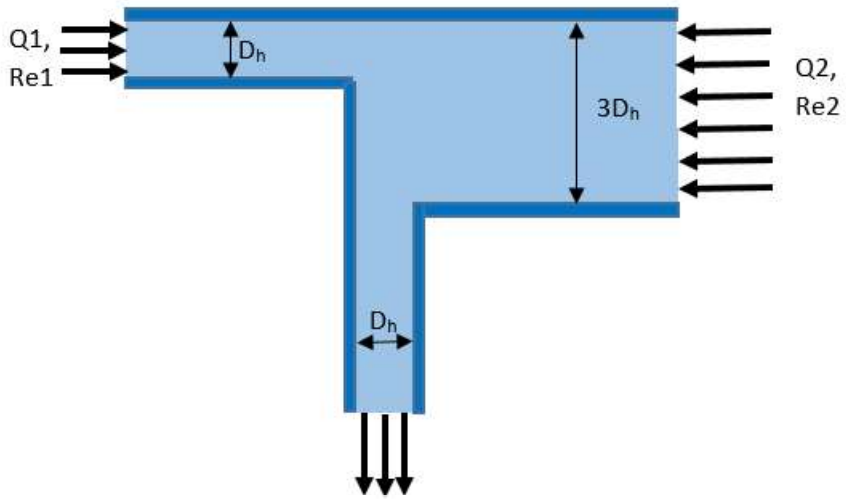

Figure 4: A Model Geometry with Different D_h

Table 9 shows this model's naming convention.

Table 9: Naming Convention for the Additional Model

Parameters	Result	Model Name
Q1=Q2	*Re1=2*Re2*	FR2w1
Re1=Re2	*Q1=2*Q2*	FR1w2

After determining the models, two sets of geometries were created in *SolidWorks*®. One was created at the macro scale such that

$$1D_h = 25.4\ mm$$

And the other (microscale model) is defined by:

$$1D_h = 25.4\ \mu m$$

The macro models and the micro models were created for each geometry type to explore the effect of scale on the results. The experimental parameters are presented in *Table 10.*

Table 10: Fluid Properties

Parameter	Value
Range of Reynolds Numbers	0.1-100
Diffusivity (m^2s^{-1})	$2.68*10^{-9}$
Density ($kg*m^{-3}$)	998.2
Viscosity (Pa*s)	0.001003
Temperature (K)	300

III. 3 Grid Independence Study

After construction of the geometries, they were meshed using *ICEM CFD*™. To determine the quality of the mesh, as well to determine where mesh refinement should occur, an open source visualization software, *VisIt*™, was utilized. A mesh was determined to be sufficient when the plot of the velocity magnitude was smooth for the entire range of Reynolds numbers, and the centerline velocity magnitude was equal to the theoretical center line velocity for a square duct determined by:

$$v_{centerline} = \frac{2Re\mu}{D_h\boldsymbol{\rho}} \qquad 34$$

Additionally, the velocity profile at the midplane was compared to the theoretical velocity profile at the appropriate Reynolds number for a square duct. The first mesh was a tetrahedral mesh with refinements at the faces and edges. The corresponding velocity magnitude plot are shown in *Figure 5* for an arbitrary test case.

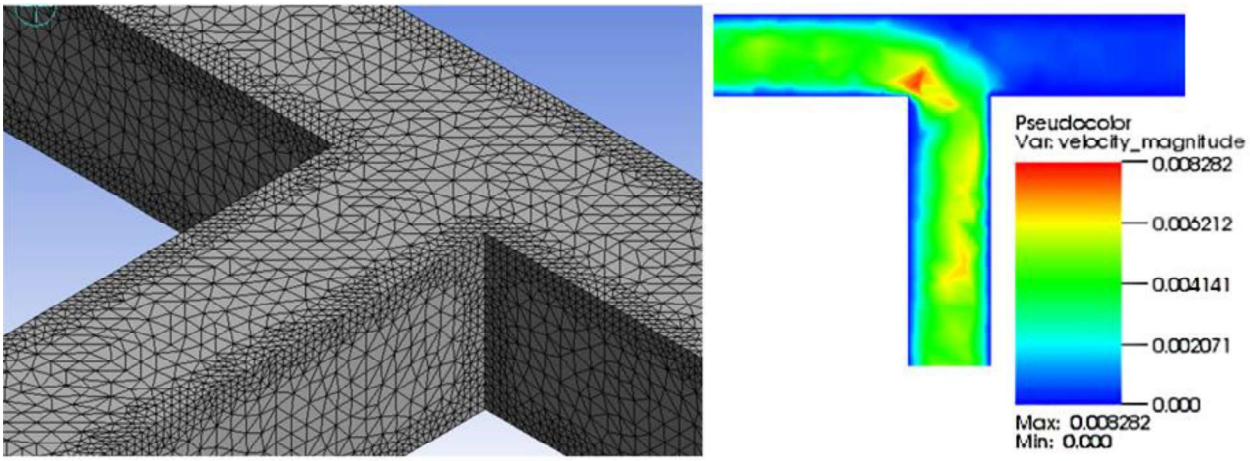

Figure 5: Non-Uniform Tetrahedral Mesh with Refinements

Clearly, the solution is not continuous, so a uniform hexahedral mesh was selected (*Figure 6*). Just as in *Figure 5* the solution is not continuous, but it is improved. In pursuit of a sufficient uniform hexahedral mesh, first the centerline velocity profiles were compared (*Figure 8*). The result for this approach are outlined below in *Table 11*. A comparison of the first (*Figure 6*) and final mesh (*Figure* 7) iterations and their corresponding pseudocolor plots are shown.

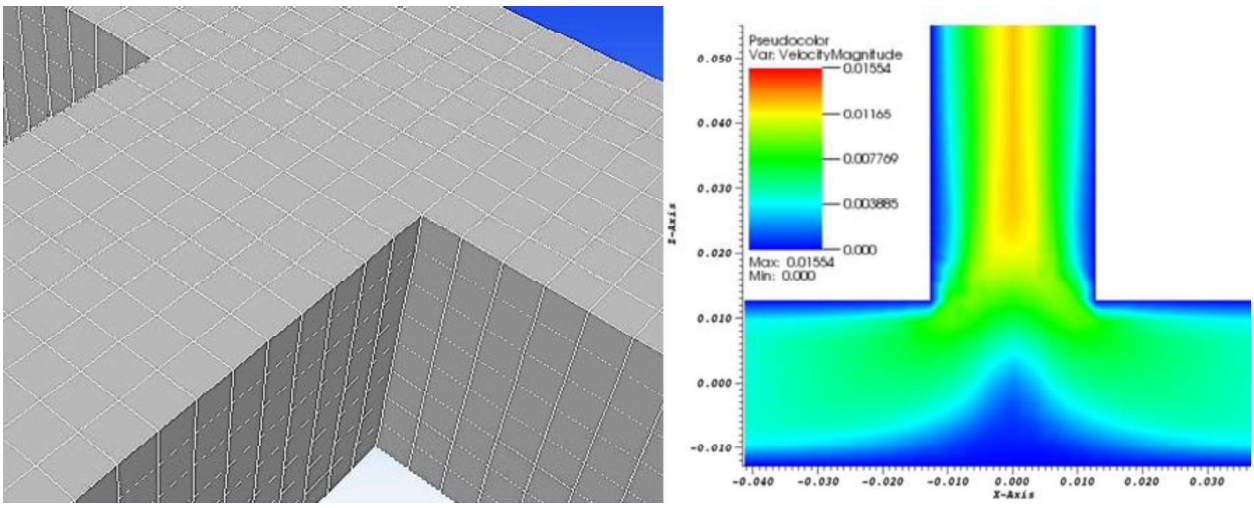

Figure 6: First Uniform Hexahedral Mesh

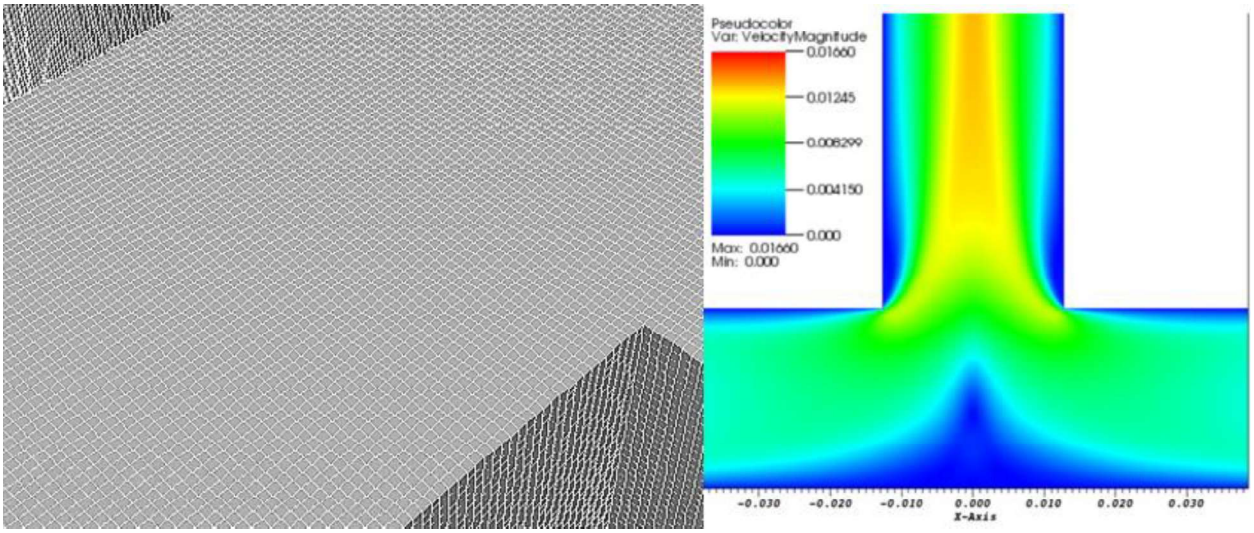

Figure 7: Final Uniform Hexahedral Mesh

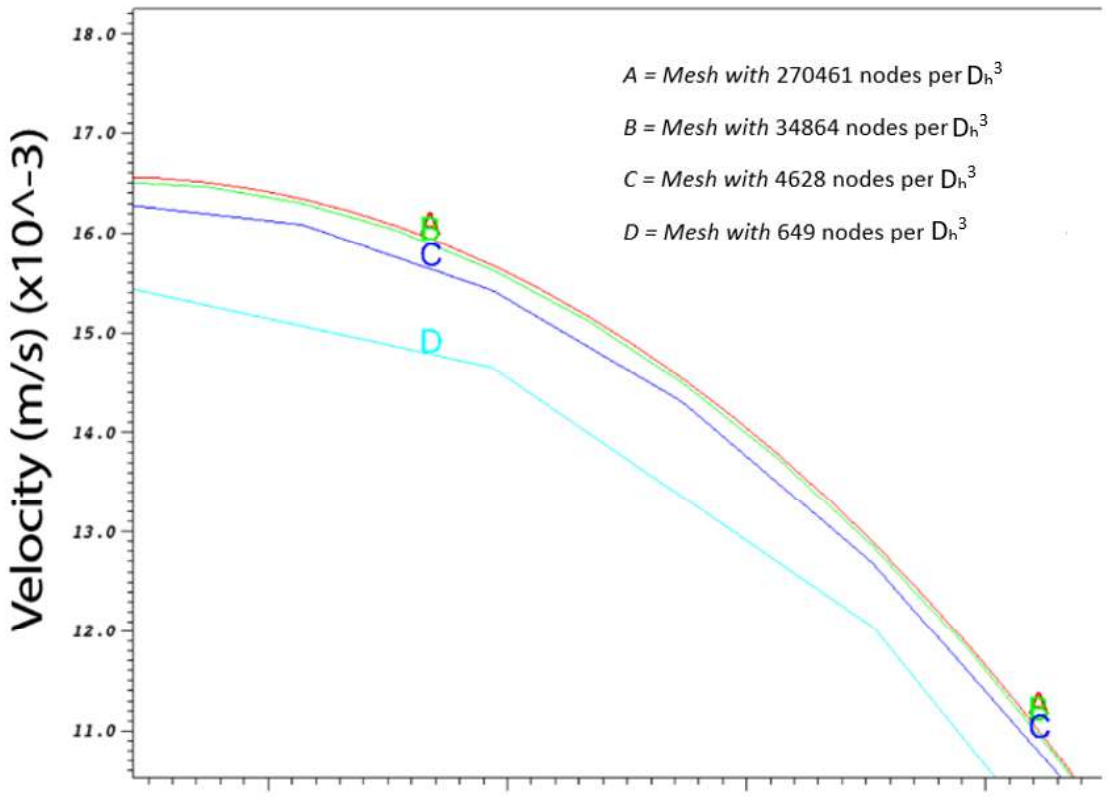

Figure 8: Centerline Profiles for the Meshes 1-4

Table 11: Grid Independence Study 1

	Mesh 1	Mesh 2	Mesh 3	Mesh 4
Max Edge Length (L/Dh)	0.125	0.0625	0.03125	0.015625
Nodes per 1Dh^3 Volume	649	4628	34864	270461
Maximum Centerline Velocity (m/s)	1.545E-02	1.627E-02	1.650E-02	1.655E-02
%Difference (Mesh N, N-1)	----------	5.15%	1.42%	0.30%

Due to the diversity of the quantities being considered, this study was expanded to include the viscous term of the entropy generation rate and the standard deviation of the mass fraction. These results are outline in *Table 12.* The study was conducted for a range of Reynolds numbers and

flow weighting to track the effect that each term independently has on the solution. The final mesh, as determined by the grid independence study, has 270461 nodes per $1Dh^3$.

Table 12: Grid Independence Study 2

w11							
	Mesh 1	Mesh 2	Mesh 3	Mesh 4	$\%Diff_{12}$	$\%Diff_{23}$	$\%Diff_{34}$
Nodes	44793	319345	2405601	18661825	---	---	---
$\dot{S}_f$	1.43E-09	1.79E-09	1.93E-09	1.99E-09	19.94%	7.41%	2.76%
$\sigma_{massFraction}$	0.4701060653	0.481484417	0.4845691712	0.4824115695	2.36%	0.64%	0.45%
w12							
	Mesh 1	Mesh 2	Mesh 3	Mesh 4	$\%Diff_{12}$	$\%Diff_{23}$	$\%Diff_{34}$
Nodes	44793	319345	2405601	18661825	---	---	---
$\dot{S}_f$	6.55E-10	8.05E-10	8.64E-10	8.91E-10	18.58%	6.82%	3.02%
$\sigma_{massFraction}$	0.3297863902	0.3790009577	0.4271677498	0.451705293	12.99%	11.28%	5.43%
w14							
	Mesh 1	Mesh 2	Mesh 3	Mesh 4	$\%Diff_{12}$	$\%Diff_{23}$	$\%Diff_{34}$
Nodes	44793	319345	2405601	18661825	---	---	---
$\dot{S}_f$	4.16E-10	5.26E-10	5.69E-10	5.87E-10	20.95%	7.45%	3.13%
$\sigma_{massFraction}$	0.2072995137	0.3442044608	0.4065826204	0.4351929383	39.77%	15.34%	6.57%

Chapter IV: Results

To best understand the results, a key describing the flow cases is provided below. The key is generated from the naming convention developed in *Chapter III*.

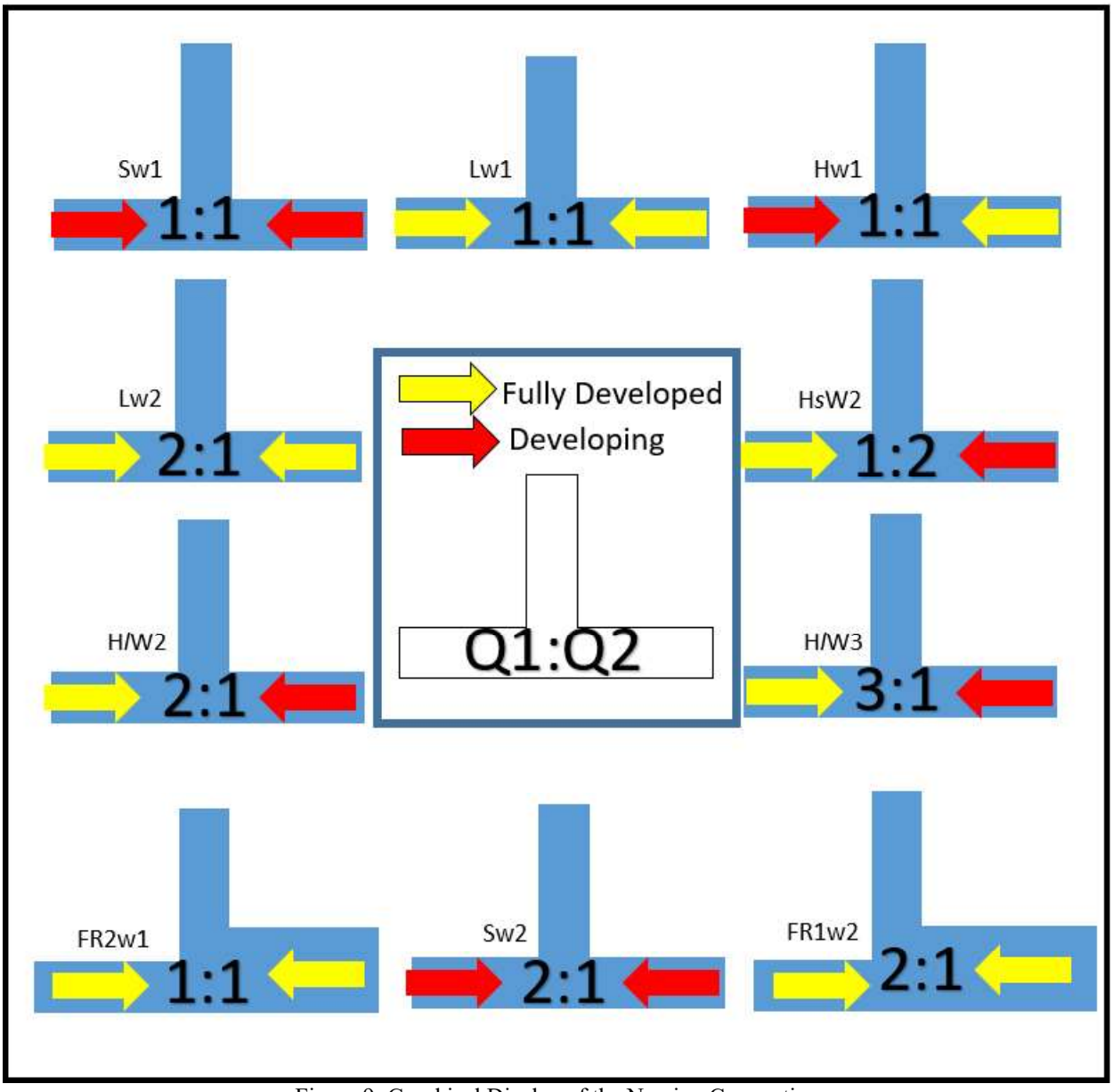

Figure 9: Graphical Display of the Naming Convention

IV.1 Mixing Efficiency versus Reynolds

In developing a functional relationship between the mixing efficiency and Reynolds number, simulations had to be conducted for a wide range of Reynolds number for every flow case in question.

IV.1.1 Preliminary Results

First, using *VisIt*™, the mixing index was calculated using *Equations 7-8.* The calculations were done at several outgoing cross sections. The result yields a better understanding of the relationship between the mixing efficiency and the Reynolds numbers as it relates to residence time of the fluid in the channel. The plots for each flow case are provided in *Figure 10-13*, and larger versions are in *Appendix I.*

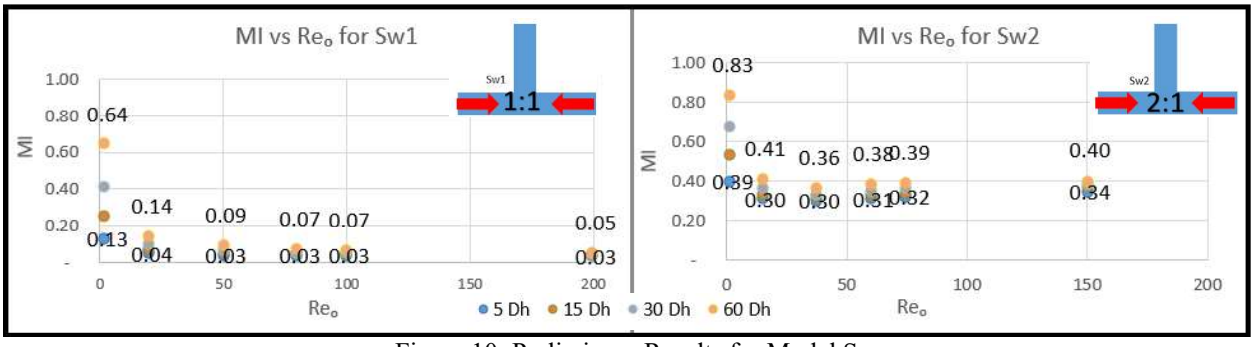

Figure 10: Preliminary Results for Model S

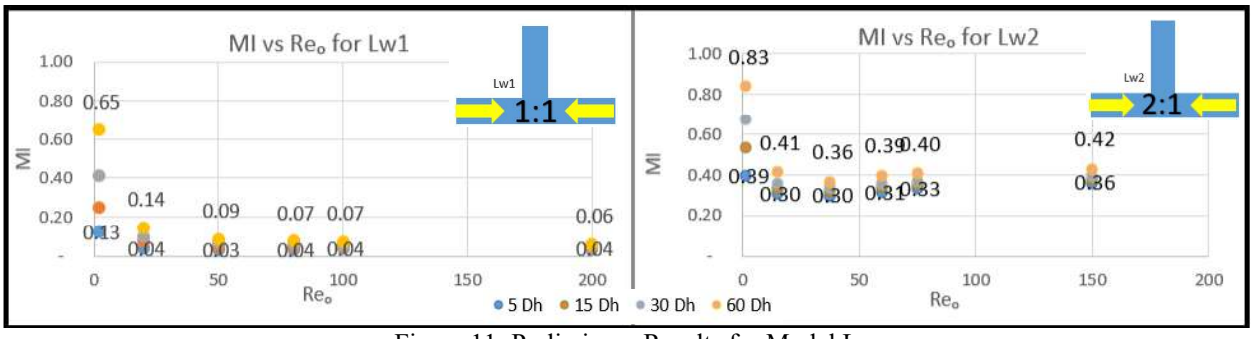

Figure 11: Preliminary Results for Model L

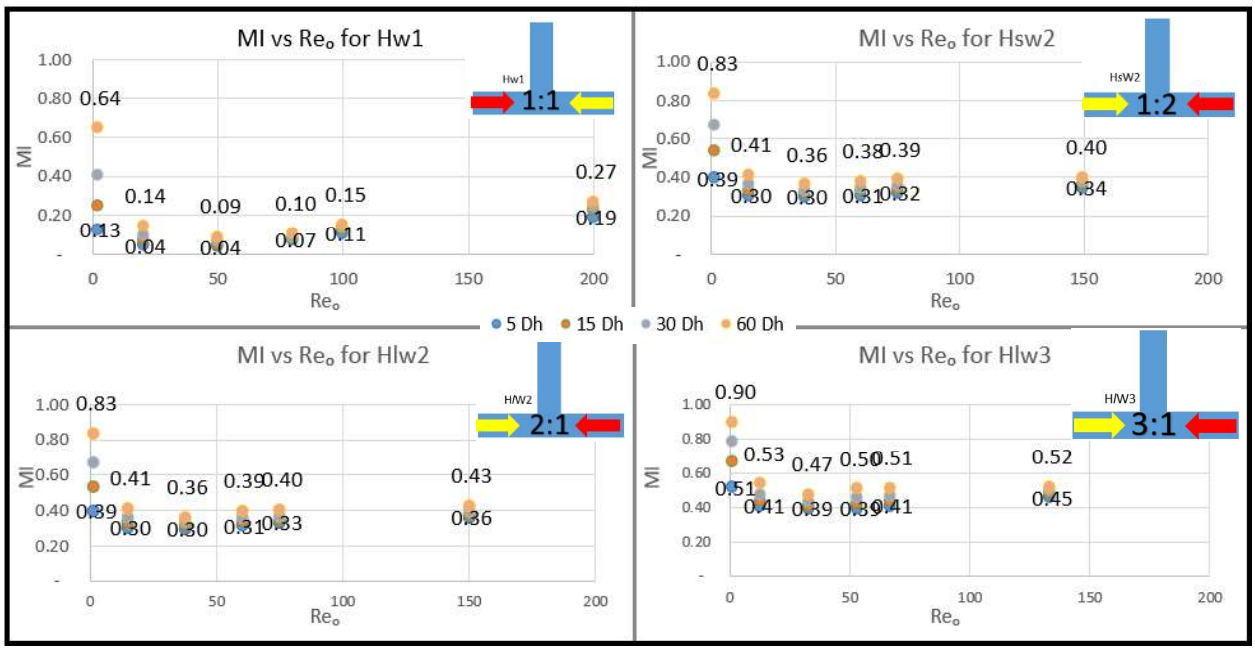

Figure 12: Preliminary Results for Model H

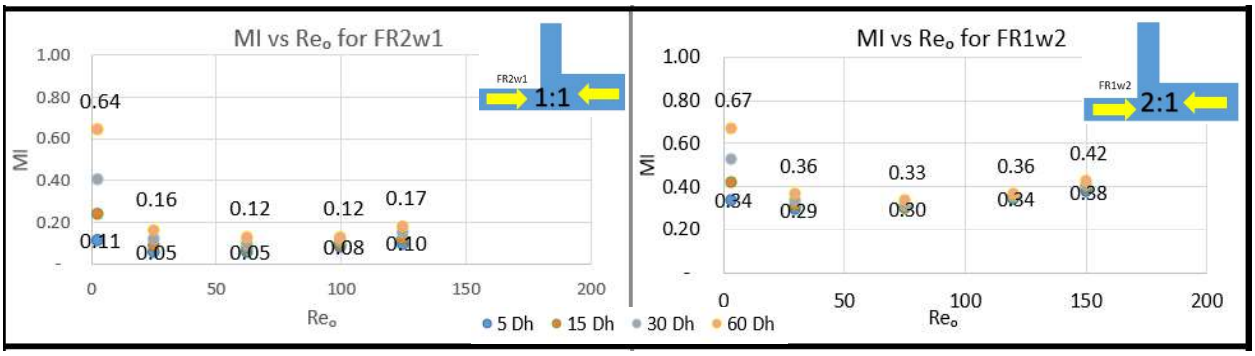

Figure 13: Preliminary Results for Model F

IV.1.2 Preliminary Conclusions

From *Figure 10-13,* there are a few conclusions that help to guide the remainder of the simulations and results for the thesis. These conclusions are outlined as follows:

1. Flow asymmetry in the form of differing flow weights (see models with $w_f > 1$), or in the form of how developed a fluid is (Hw1 > Lw1), promotes mixing in a tee shaped micromixer.

2. Assuming the fluids have different flow weightings, at a minimum the faster branch should be fully developed. The other branch can be developing or fully developed with no impact on mixing efficiency (Hlw2 > Hsw2).
3. Increased flow weighting increases mixing efficiency.
4. Branch width has little effect on the mixing efficiency when compared to the flow rates of the fluid (FR1w2 > FR2w1). Thus, the mixing efficiency is driven mostly by flow rate, rather than Reynolds number at a given flow rate.

Additionally, an important observation can be made. Clearly, at the lower Reynolds numbers, the mixing efficiency appears to be abnormally high. However, when considering the two modes of mixing: chaotic advection and diffusion. The driving mechanism for mixing at the lowest Reynolds numbers is the diffusion, as evidenced by the spacing of the results at different downstream diameters. Conversely, at the higher Reynolds numbers, the downstream distance has little impact, due to the low residence time of the fluid in the mixer. As mentioned previously, it is not practical to rely on diffusion as the mode of mixing for most applications, so the diffusive impact needs to be removed, and the chaotic advection focused on. *Figure 14-16* show the modes of mixing to be lamination and chaotic advection generated simply through changing the flow weightings.

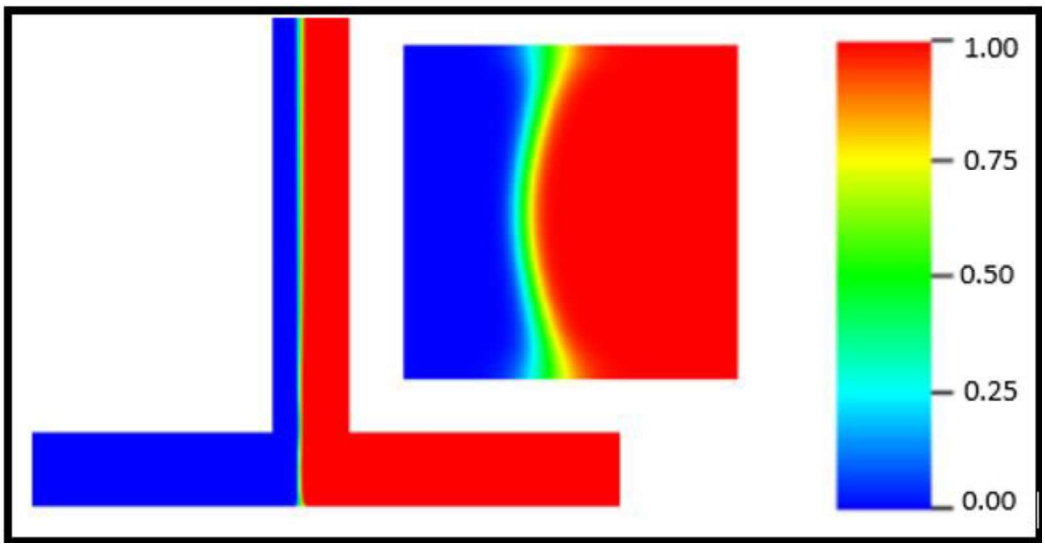

Figure 14:Plot of Mass Fractions for Hlw2 Re=5 at the midplane (Left) and Outgoing Cross Section (Right) at 5 Dh

Notice that for low Reynolds number flows, with close to symmetric flow weightings yields undesirable mixing efficiencies. However, with increased flow weighting, the contact area, and thus the mixing efficiency greatly improves (*Figure 15*).

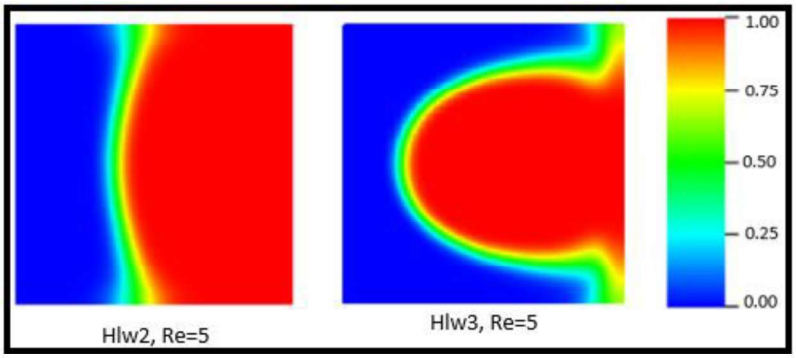

Figure 15: Comparison of Mass Fraction Plots for Different Flow Weightings at 5 D_h.

To increase the chaotic advection then, the combination of increasing flow weighting and increasing Reynolds number can enhance secondary flows and contact areas thus improving mixing.

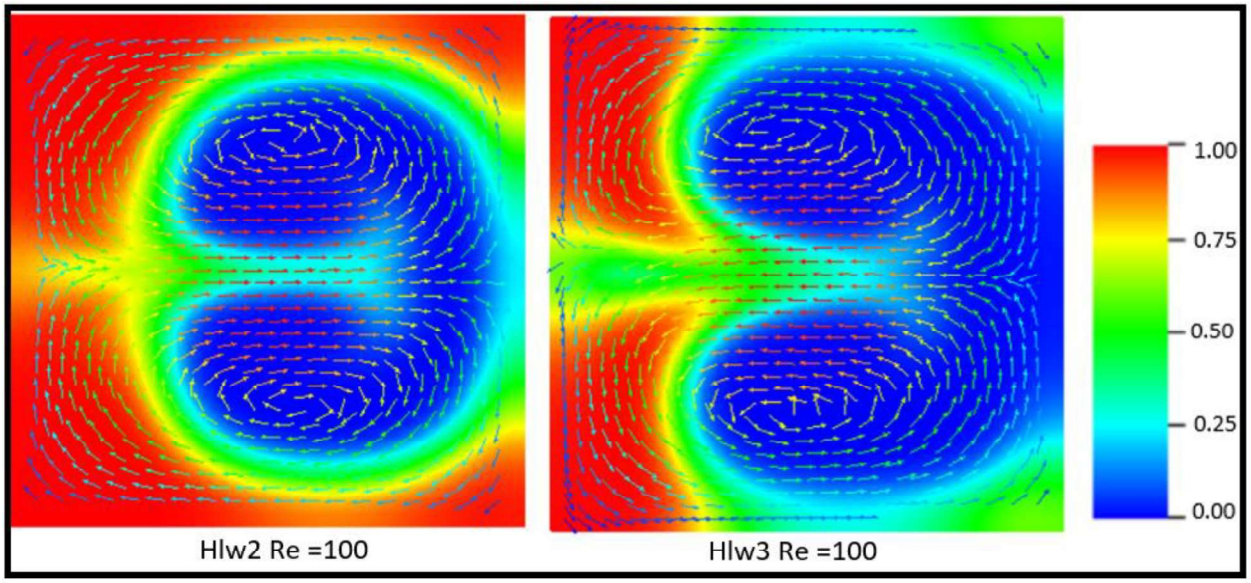

Figure 16: Comparing Flow Weightings at Higher Reynolds with Vectors Showing Secondary Flows at 5 D_h.

IV.1.3 A Modified Approach

To focus on the effect of the chaotic advection part of the mixing, the residence time has to be shortened for all flow cases for which the diffusion has a larger impact. To do this is in a standardized manner, the diffusion must be considered at the molecular level. For a stationary fluid, the time for a single molecule to diffuse through a fluid is given by:

$$t_{diff} = \frac{stl(0)^2}{2D} \tag{35}$$

Where *stl(0)* is the striation length. For complete mixing by diffusion, the striation length would be equivalent to the farthest distance a molecule would have to travel to mix into the other fluid. For the case of two entirely unmixed fluids with equal flow weight meeting in a tee junction, this distance would be equal to half of the hydraulic diameter of outgoing pipe. However, this time is hardly relevant if the scale is changed, so non-dimensionalizing *Equation 36* leads to:

$$t^*_{diff} = \frac{t_{diff} * v_o}{D_h} = \frac{Re * \mu}{8D\rho} \tag{36}$$

Therefore, to lessen the residence time, we need to take 0.1% of the total time such that,

$$t^* = 0.001 * t^*_{diff} \quad (37)$$

This equation, however, is more useful when considering the length that the fluid would travel during this time. Rearranging:

$$L_{out} = \frac{0.001 * D_h^2}{8D} v_o \quad (38)$$

Taking the mixing efficiency at the cross section for this distance will isolate the chaotic advection in the mixing results. For the remainder of the results, all mixing efficiencies and volumetric entropy generation terms will be bounded by L_{out} as illustrated by *Figure 17.*

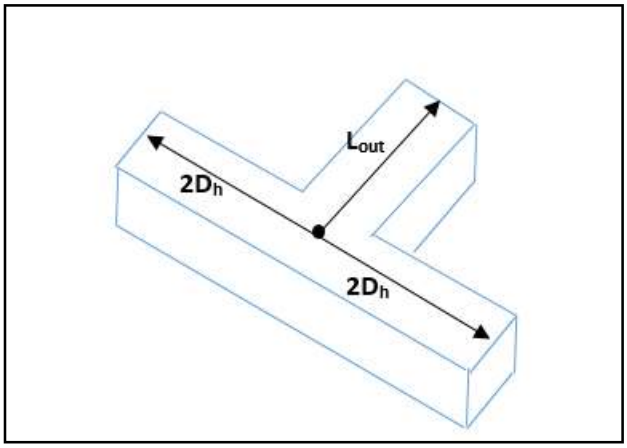

Figure 17: Schematic Demonstrating the Determination of L_{out}

Using this approach and revisiting the mixing efficiencies yields the results in

Figure 18.

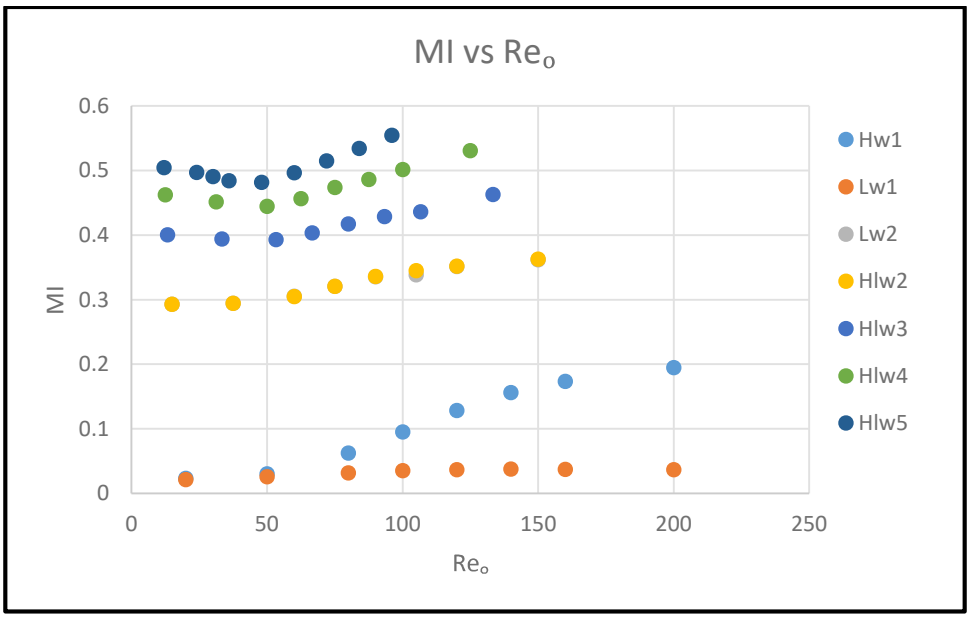

Figure 18: Mixing Index vs Re_o at t^*.

Clearly the observed effect of the diffusion portion has been lessened, though not completely eliminated, simply due to the fact that at lower Reynolds, the driving term is almost exclusively diffusion. Additionally, one should note that with the exception of the *Hw1* plot, the shape of the curves is consistent leading to the conclusion that 1) when asymmetry is created through developing flow alone, there are other factors for mixing that should be accounted for, and 2) one could seek a relationship that is independent of flow weighting to derive a general analytical expression. The form of the equation will be:

$$MI * P = \xi * Re + \omega \tag{39}$$

Where P is some non-dimensional normalizing function and ξ and ω are constants to be determined. The desired form of P would be a function whose value can be determined for other flow cases other than those that are presented here, such that:

$$P = f(w_f) \tag{40}$$

However, in the case of unity w_f a relationship should be sought in the realm of other relevant parameters, such that:

$$P_{w_f=1} = f(Re) \tag{41}$$

Using these two functions the following is determined:

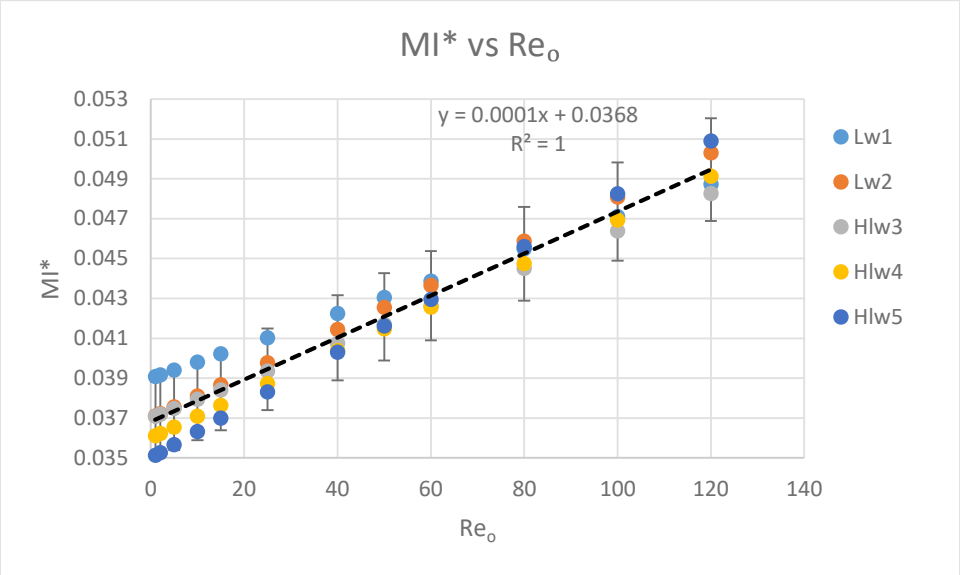

Figure 19: Graphical Determination of the Normalized Analytical Relationship

The analytical relationships that arise are:

$$MI^* = MI * P = (1.055x10^{-4}Re_o + 0.037) \pm 2\sigma \tag{42}$$

Where:

$$P = \left(-14.594(w_f + 1)^{\frac{1}{w_f}} + 32.412\right)^{-1} \tag{43}$$

And

$$P_{w_f=1} = 6.434x10^{-5}Re_o^2 - 0.016Re + 2.317 \tag{44}$$

The developed analytical relationships are independent of scale and applicable for any w_f including non-integer values. Additionally, it should be noted that this particular relationship

only holds for this particular geometry or similar geometries as demonstrated by this thesis. However, this process can be followed to develop similar relationships for any mixer.

IV.1.4 Comparing Micro and Macro Scale

When considering the mixing efficiency for the micro scale, it is helpful to first anticipate the results by analyzing the definition of t^* and L_{out}. Looking at these parameters, it is clear that the decrease in contact area developed by the smaller scales is compensated by the increase in the length that the fluid interacts over. Interestingly, the increase in velocity that occurs for decreased channel hydraulic diameter at a constant Reynolds number, leads to a proportional increase in chaotic advection over the increased length to that lost in the fluid area over which advection could have occurred. However, the increase in velocity also makes it difficult to obtain convergence for some of the higher Reynolds numbers, though the collected data is sufficient to justify the result. This is seen in the comparison of the results for full and micro scale models in *Figure 20.*

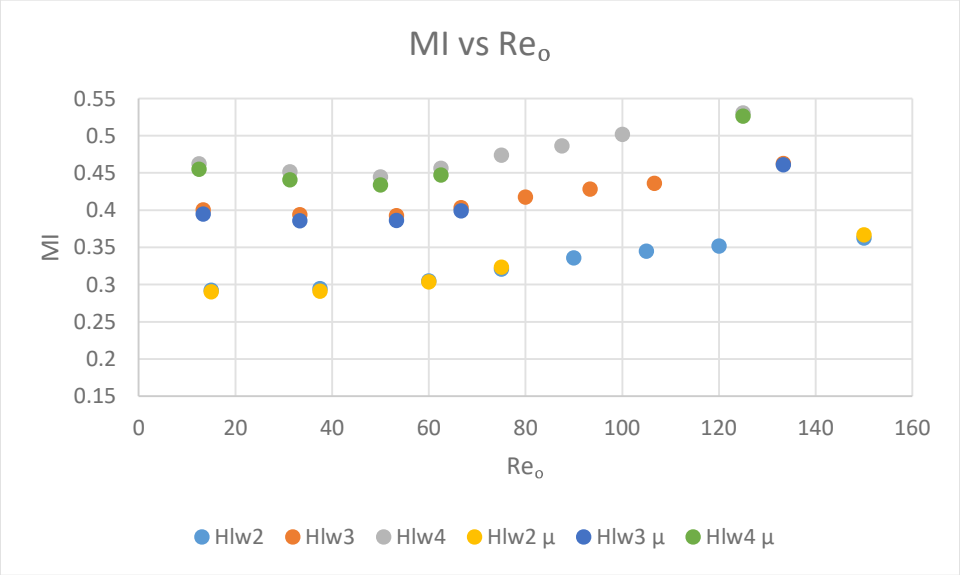

Figure 20: Graphical Comparison of Full and Microscale MI

Therefore, it can be concluded that mixing efficiency when determined using this method is independent of scale, so the analytical relationships developed for the full scale model are applicable for any scale.

IV. 2 Summary of Mixing Efficiency improvement.

Having conducted the analysis for a range of models, using several methods it is helpful to consider the results as a whole. *Table 13* provides the mixing lengths and indices for pure diffusion (independent of Reynolds number, see *Equation 36*), pure chaotic advection (*Equation 43*), and a combination of both diffusion and chaotic advection (*Chapter IV.1.1*).

Table 13: Summary of Mixing Efficiencies and Lengths for mixing Constituents at w_f=1

w1							
		Pure Diffusion		Pure Chaotic Advection		Combined	
Re_{in}	Re_o	Mixing Length(Dh)	MI	Mixing Length(Dh)	MI	Mixing Length(Dh)	MI
1	2	9.37E+01	1	9.37E-02	0.016	30	0.411
10	20	9.37E+02	1	9.37E-01	0.019	30	0.098
25	50	2.34E+03	1	2.34E+00	0.025	30	0.064
50	100	4.69E+03	1	4.69E+00	0.035	30	0.055
100	200	9.37E+03	1	9.37E+00	0.034	30	0.047

Table 14: Summary of Mixing Efficiencies and Lengths for mixing Constituents at w_f=2

w2							
		Pure Diffusion		Pure Chaotic Advection		Combined	
Re_{in}	Re_o	Mixing Length(Dh)	MI	Mixing Length(Dh)	MI	Mixing Length(Dh)	MI
1	1.5	3.12E+01	1	7.03E-02	0.27	30	0.67
10	15	3.12E+02	1	7.03E-01	0.28	30	0.36
25	37.5	7.81E+02	1	1.76E+00	0.29	30	0.33
50	75	1.56E+03	1	3.51E+00	0.32	30	0.37
100	150	3.12E+03	1	7.03E+00	0.35	30	0.39

Table 15: Summary of Mixing Efficiencies and Lengths for mixing Constituents at w_f=3

w3							
		Pure Diffusion		Pure Chaotic Advection		Combined	
Re_{in}	Re_o	Mixing Length(Dh)	MI	Mixing Length(Dh)	MI	Mixing Length(Dh)	MI
1	1.3333	1.56E+01	1	6.25E-02	0.39	30	0.78
10	13.3333	1.56E+02	1	6.25E-01	0.41	30	0.47
25	33.33333	3.91E+02	1	1.56E+00	0.43	30	0.44
50	66.66666667	7.81E+02	1	3.12E+00	0.47	30	0.47
100	133.3333333	1.56E+03	1	6.25E+00	0.51	30	0.51

Clearly for lower Reynolds numbers, the mixing relies most heavily on the diffusion, though the mixing times are impractical. Thus, to increase the mixing, chaotic advection should be invoked through the use of flow weight differences. As seen here, using this technique, the mixing lengths are shortened dramatically with a sharp increase in mixing efficiency. In practical

applications this means that the method developed here in this thesis can noticeably increase mixing efficiency within a shorter mixer, thus satisfying the goal of practical micromixer designs.

IV.3 Entropy versus Reynolds

The next objective to be accomplished is finding an analytical relationship between non-dimensionalized entropy generation rate (*Equation 19*) for the volume discussed (*Figure 17*) previously as a function of the outgoing Reynolds number.

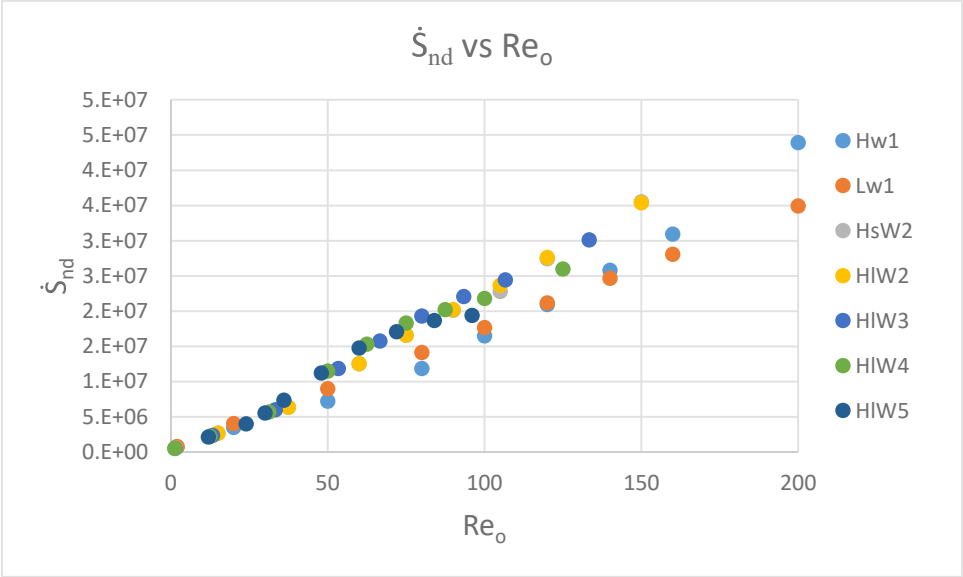

Figure 21: Comparing Non-dimensionalized Entropy Generation Rates for Various Flow Cases at the Full Scale.

It is immediately apparent that entropy generation is linearly related to the outgoing Reynolds number for this scale. However, when considering the micro scale another relationship emerges.

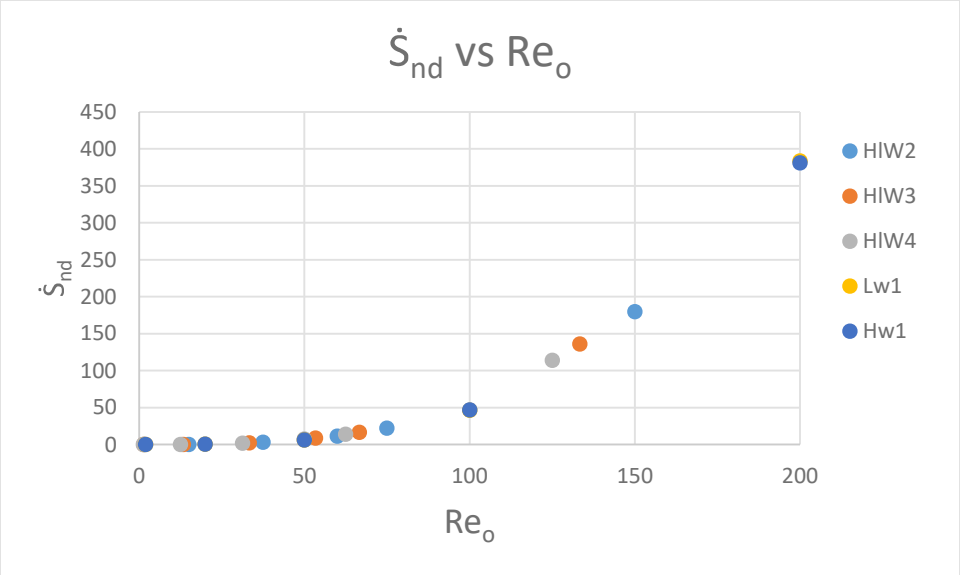

Figure 22:Comparing Non-dimensionalized Entropy Generation Rates for Various Flow Cases at the Micro Scale.

Looking at the plots, two differences arise, scale and shape. For the total non-dimensionalized entropy generation, scale does impact the values. This could have been hypothesized considering the relative differences in γ_1 and γ_2 from *Equations 23* and *24*. So looking at the terms individually yields *Figure 23*.

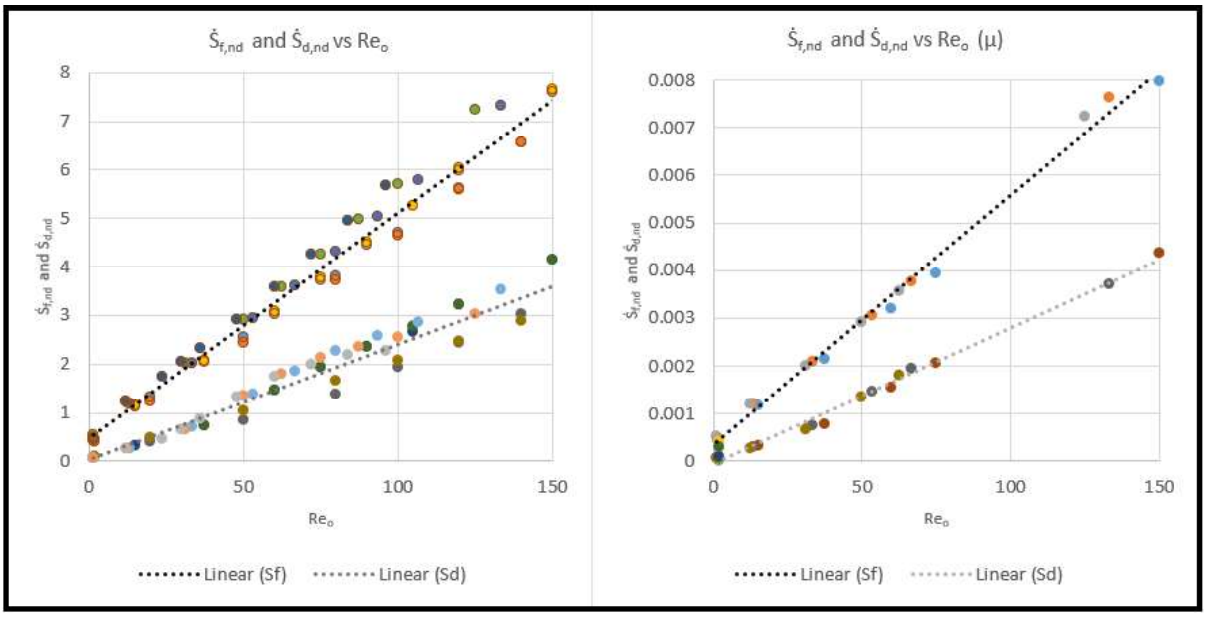

Figure 23: Comparing Full and Micro Scale Entropy Generation Rates

Comparing both scales above, one can develop the analytical relationships for the diffusive and viscous entropy generation terms separately.

$$\frac{(\dot{S}_{F,nd})}{SF} = (0.052Re_o + 0.338) \pm 2\sigma \quad 45$$

$$\frac{(\dot{S}_{D,nd})}{SF} = (0.026Re_o + 0.033) \pm 2\sigma \quad 46$$

Where *SF=0.01* in standard SI units, and scaling down decreases *SF* accordingly.

Table 16: Determination of SF

Scale of the Model (1 for SI)	SF
$k(10^3)$	100000
$1(10^0)$	100
$c(10^{-2})$	1
$m(10^{-3})$	0.1
$\mu(10^{-6})$	0.0001

IV. 4 Entropy Generation versus Mixing Efficiency

This thesis hypothesized an analytical relationship between the mixing efficiency and the entropy generation for a micromixer. A main goal of this thesis was to demonstrate such a relationship. By taking the approach of developed in *Chapter IV.1.*3 and using similar analytical relationships between each quantity and the outgoing Reynolds number, the final analytical proof is straight forward. Because this thesis recognized the necessity of decomposing the entropy generation rates into its relative parts, the same format can be used to express the developed analytical relationships.

$$\frac{(\dot{S}_{f,nd})}{SF} = (492.891MI^* - 17.899) \pm \sigma \quad 47$$

$$\frac{(\dot{S}_{D,nd})}{SF} = (246.44MI^* - 9.085) \pm \sigma \quad 48$$

The developed analytical relationships are devoid of scale, and are strictly applicable to this particular set of micromixers, though it holds for any flow parameters within those geometries. This procedure could of course be followed for any micromixers, and similar relationships be developed, making this work even broader than the specifically presented results.

Chapter V: Application

V.1 Validation of Shih and Chung's Results

Shih and Chung [7] attempted to develop a high efficiency planar passive micromixer by combining multiple types of individual micromixers. Specifically, their micromixer is designed to take advantage of injection mixing and increased chaotic advection through the placement of obstacles. Their design was selected for the ease of fabrication and the wide range of applicable Reynolds numbers. Their micromixers produce a mixing efficiency at the outlet greater than 85 percent. For this reason, their micromixer has been selected as a starting point for applying the preliminary conclusions reached in *Chapter IV* in the creation of a better micromixer.

V.1.1 Model Formulation and Grid Independence Study

First, consider the model that Shih and Chung developed. Through the use of the Taguchi method two separate designs were created. The models have been reproduced to specification.

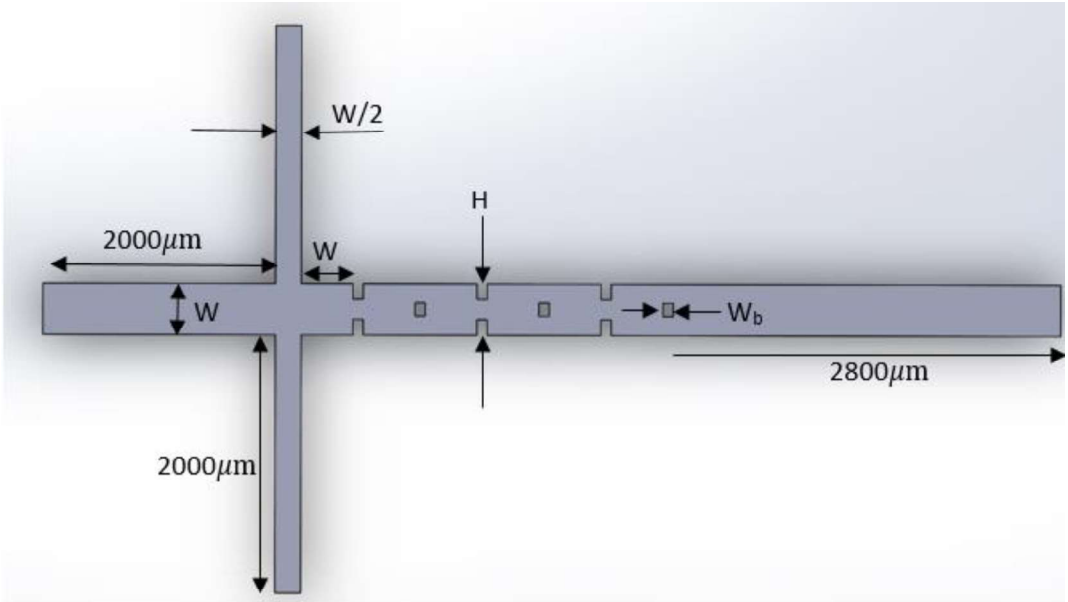

Figure 24: Model Developed by Shih and Chung

In *Figure 24:*

$$W = 400\mu m$$

$$H = W * G$$

$$W_b = 80\mu m$$

G is defined as the gap-ratio where the gap would have thickness *H*. The overall thickness of the model is 120µm. The two cases being explored are:

$$G = \frac{1}{8}\ and\ \frac{3}{8}$$

To better define the necessary mixing lengths for each model (the length that is necessary to achieve the desired mixing efficiency), the model is further defined to include the locations outlined in *Figure 25*.

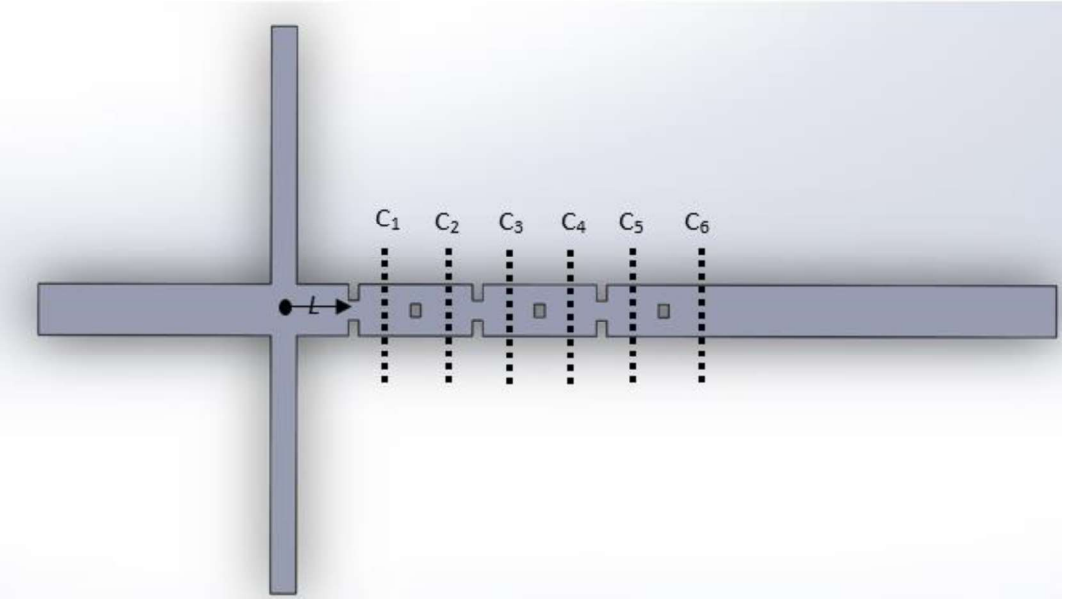

Figure 25: Defining Locations for Analysis

The locations of C_i are taken midway through the respective *mixing units*, where a mixing unit is a portion of the micromixer through which a change in geometry promotes mixing. *Table 17* defines the location of these mixing units in the units appropriate to the developed model.

Table 17: Definition of Cross Section Locations

Location	Distance L (μm)
C_1	780
C_2	1260
C_3	1740
C_4	2220
C_5	2700
C_6	3180

To conduct the analysis to the specifications outlined in Shih and Chung [7], the fluid parameters in *Table 18* were utilized. Though the temperature was not specified for this analysis, the same assumed conditions and boundary conditions as in the previous sections of this thesis were applied (non-slip, isothermal, and outflow), providing the same method for analysis, yielding results that are independent of temperature.

Table 18: Experimental Parameters for Design of a High Efficiency Micromixer

Parameter	Value
Range of Reynolds Numbers	0.1-100
Diffusivity (m^2s^{-1})	$3.23*10^{-10}$
Density ($kg*m^{-3}$)	998
Viscosity (Pa*s)	0.00089

V.1.2 Preliminary Results

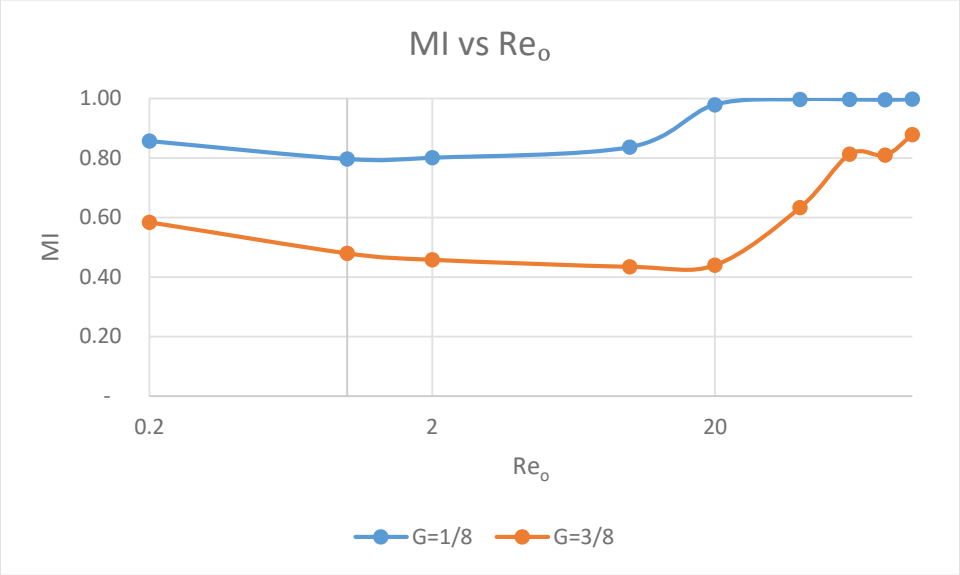

Figure 26: Validation of Shih and Chung

Just as in [7] lower Reynolds numbers show a higher mixing efficiency (driven by diffusion), with a gradual decrease through the intermediate values and a sharp climb at the higher Reynolds numbers when chaotic advection is driving the mixing. Though the trends are the same as in [7], the values differ slightly. For consistency across the thesis, the analysis is conducted for uniform Reynolds at the inlets, where Shih and Chung maintained uniform velocity. Because the side branches have half the hydraulic diameter of the perpendicular branch, Shih and Chung would have experienced an Re_o that is 1.5 times less than the results presented here, yielding a higher mixing efficiency at the lower Reynolds numbers and a lower mixing at the higher input Reynolds number, simply due to the fact that the Re_o is lower, yielding lower chaotic advection.

V.2 Analyzing the Results

The above results are consistent with those obtained by Shih and Chung, and support the idea behind the design. A micromixer that achieves high mixing efficiency for the range of Reynolds numbers from creeping to moderate laminar values, with a minimum mixing efficiency of greater than 80 percent is considered a high performance (HP) mixer. In contrast, a mixer characterized by efficiencies less than 60 percent are termed low performance (LP) mixers. These measurements were all taken at C6. However, there are a couple of things to consider about the design 1) though the design is fairly simple, there are still three inlets that each would require a micro-valve to produce the desired flow, so a simplification could be in the production of just two inlets, 2) the practicality is not justified in the context of pump head. These results merely assume, that the flows could be easily achieved, especially in the 1/8 model. The pressure heads taken through C6 are provided in *Figure 27.*

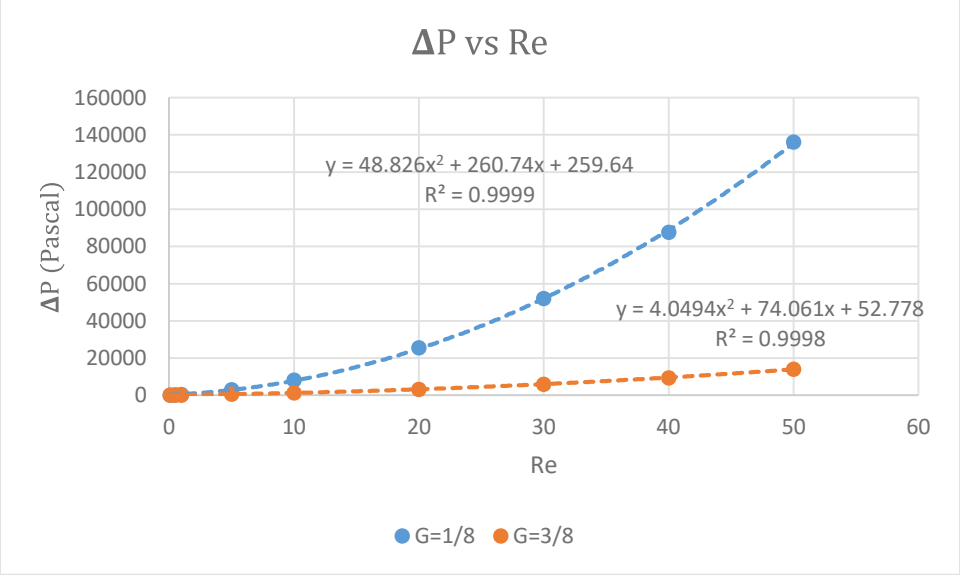

Figure 27: Analyzing the Pressure losses for the Two Designs

These results mirror those produced by Shih and Chung. However, the greater mixing efficiency for *G =1/8* comes at the cost of up to 9 times greater pumping power. This is simply avoided by the authors of [7], because they claim that relevant results are those at the lowest Reynolds numbers (less than 1), where the pressures are consistent with those found in LOC devices. However, as demonstrated by this thesis resident times for micromixers relying on diffusion are impractical.

V.3 First Iteration Improvement (Developing a "tee" Design)

In applying the work from thesis as a first iteration improvement over the micromixer developed by Shih and Chung, their specific design is simplified to include only a *tee* shaped entrance for the fluid, to eliminate the injection mixing that was originally implemented and to simplify it to include only flow weight differences. The design is given in *Figure 28.* This design only explores the gap ratio case of *G*=3/8 to seek an improvement for the LP mixer.

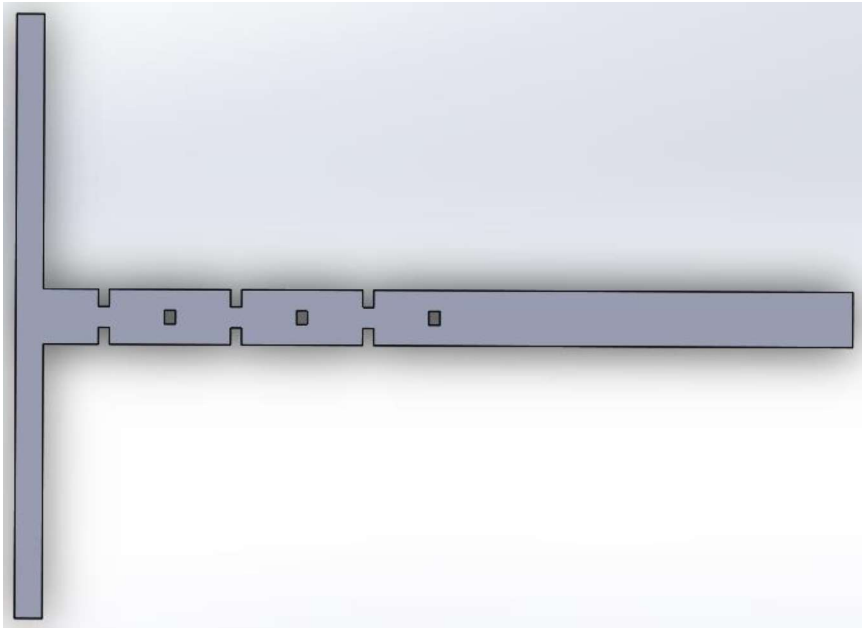

Figure 28: First Iteration Design

The other geometric design parameters remain consistent with Shih and Chung's mixer. The analysis of the relevant results is provided as follows. The naming conventions and experimental parameters are defined in *Table 19.*

Table 19: Naming Conventions

Parameter	Shih and Chung	1st Iteration Design
ΔP	Side Branch → C6	Side branch → C6
MI	Taken at C6	Taken at C6
Model Name	SC	T
Naming Suffix	Gap Ratio "*18 or 38"*	w_f *(Chapter III.2)*

Additionally, a new grid independence study was performed to ensure that the previous grid size was still applicable. As in *Chapter III.3* this study was conducted for each w_f. This analysis is displayed in *Figure 29.*

w1 Re=40									
	Mesh 1	Mesh 2	Mesh 3	Mesh 4	Mesh 5	$\%Diff_{12}$	$\%Diff_{23}$	$\%Diff_{34}$	$\%Diff_{45}$
Nodes	27015	206350	1530032	11455488	89784399	--------	--------	--------	--------
$\dot{S}_f$	1.87E-07	4.01E-07	8.41E-07	1.12E-06	1.21E-06	53.37%	52.32%	24.91%	7.44%
ΔP	30559.30	32292.63	37325.41037	37709.8385	37351.10	5.37%	13.48%	1.02%	0.96%
MI	0.985274	0.973990	0.800981456	0.82204032	0.744535	1.16%	21.60%	2.56%	10.41%

w2 Re=50							
	Mesh 1	Mesh 2	Mesh 3	Mesh 4	$\%Diff_{12}$	$\%Diff_{23}$	$\%Diff_{34}$
Nodes	27015	206350	1530032	11455488	--------	--------	--------
$\dot{S}_f$	1.62E-07	3.49E-07	6.87E-07	9.03E-07	53.58%	49.20%	23.92%
ΔP	26967.38	28644.05	32669.07392	33149.5730	5.85%	12.32%	1.45%
MI	0.989818	0.978624	0.944842786	0.92673761	1.14%	3.58%	1.95%

w10 Re=50									
	Mesh 1	Mesh 2	Mesh 3	Mesh 4	Mesh 5	$\%Diff_{12}$	$\%Diff_{23}$	$\%Diff_{34}$	$\%Diff_{45}$
Nodes	27015	206350	1530032	11455488	89784399	--------	--------	--------	--------
$\dot{S}_f$	8.15E-08	1.78E-07	3.25E-07	4.04E-07	4.26E-07	54.21%	45.23%	19.49%	5.24%
ΔP	14771.04	16571.54	18548.05659	18652.97	18569.4	10.87%	10.66%	0.56%	0.45%
MI	0.997110	0.992933	0.985463818	0.963402	0.94685	0.42%	0.76%	2.29%	1.75%

Figure 29: Grid Independence Study for Applied Model

The final model has 189128 nodes per $D_h{}^3$. Computational limits prohibited the pursuit of a finer mesh. The relevant quantities that were checked for convergence were the entropy generation rate, the pressure loss and mixing index. Due to the inconsistencies for w_f=1, the results for this model are considered qualitative only. However, the higher values of w_f are the most relevant to this thesis. All of the results for this *First Iteration Design* are outlined in *Figure 30.*

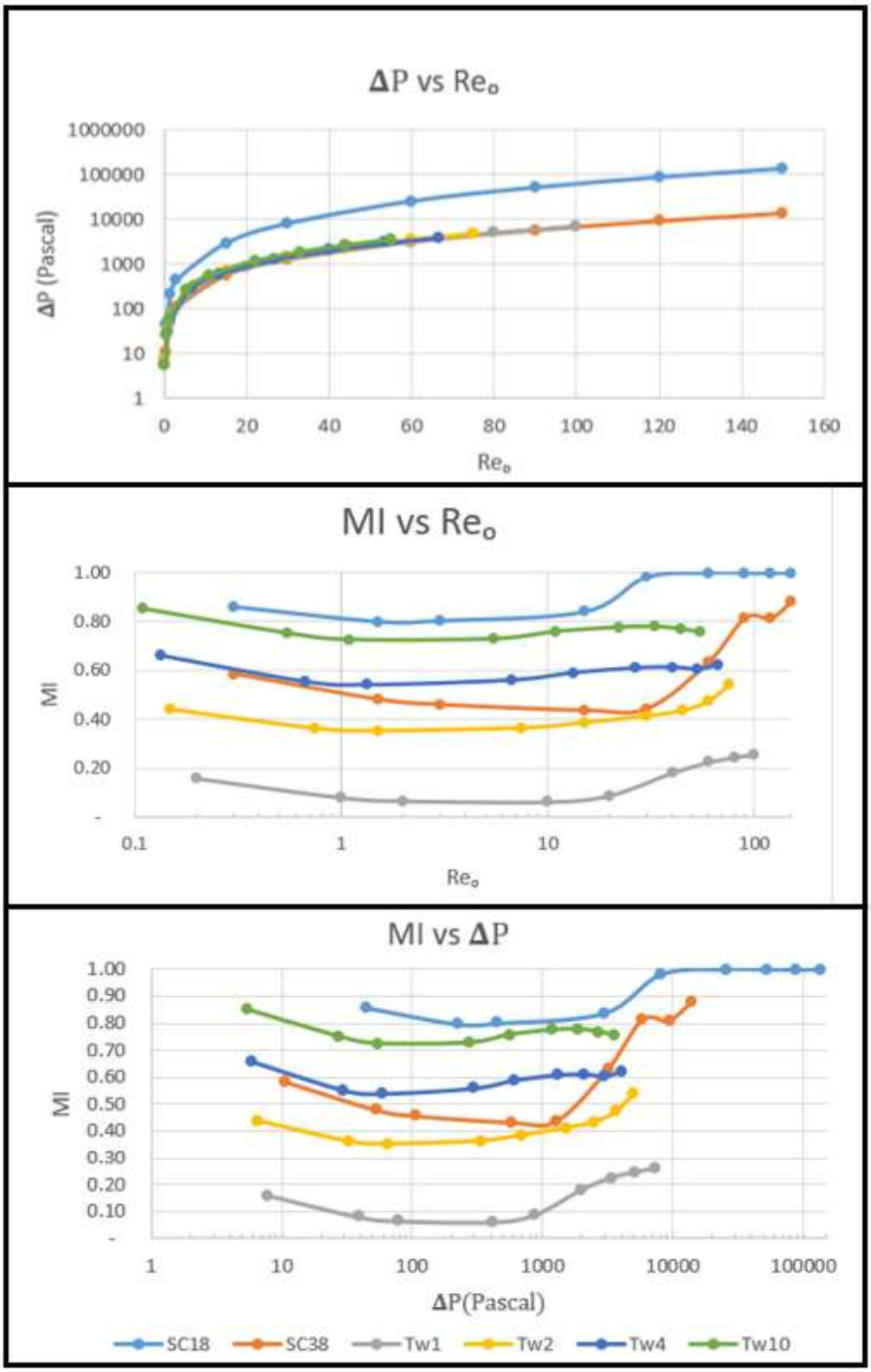

Figure 30: Comparing Results for SC vs T models at C6

From the above plots, it is clear that the obstacles are the major contributor to the pressure losses in the system, especially at the moderate to higher Reynolds numbers. Also, in looking at the mixing index, it is clear that for this *First Iteration Design* (arbitrary) mixer, increasing the flow weighting does increase the mixing index, even beyond Shih and Chung's [7]mixer, especially for higher flow weighting. In considering the midplane mass fraction distribution for Shih and Chung's micromixer, it is apparent that increasing the flow weighting, is more effective than simply relying on obstacle based mixing units. Additionally, in considering the mixing index as a function of the pressure drop, greater flow weighting contributes to a rise in mixing index of over 0.4 for the same pressure losses when comparing *Tw1* and *Tw10*. However, it is undeniable that the mixing unit obstacles do contribute to Shih and Chung's mixing efficiencies; therefore, one should then consider a mixer specifically designed to increase the mixing efficiency through flow weightings and obstacles.

V.4 Second Iteration: New Micromixing Technique

An obvious second iteration micromixer, to improve the overall mixing efficiency at a wide range of Reynolds numbers, would be one that placed obstacles in way to constructively increase the chaotic advection. Consider the modification of the previous design by simply moving the obstacles over to "catch" the shifted flow and create secondary flows. *Figure 31* demonstrates the need for placing the obstacles in a productive location. Notice the increased mixing at the corner behind the obstacles in the *SC* model when compared to the *T* model at the midplane.

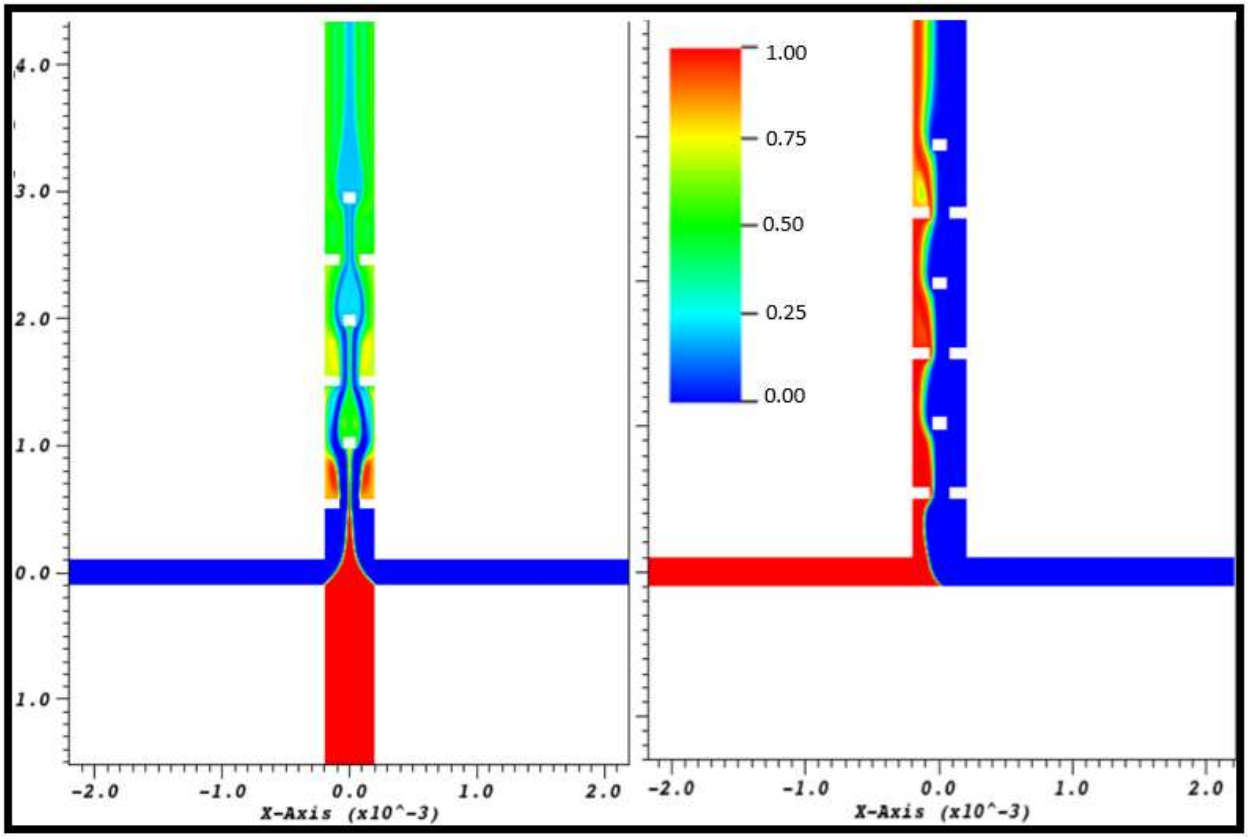

Figure 31: Comparing Mass Fraction Distributions for SC and T Models

The new model (*Figure 32*) is specifically designed to address this design consideration.

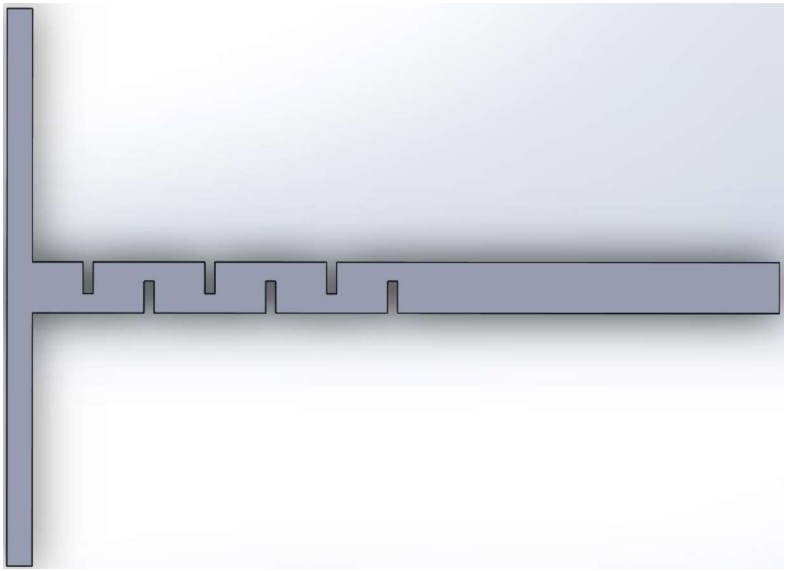

Figure 32: Second Iteration Model Design

To create a more thorough analysis of the designed micromixer, several parameters will be considered. First, the results will be considered for both locations: *C3* and *C6*. This will allow a fair determination of the practical shortest micromixer necessary to achieve the desired results. Additionally, the designed high efficiency micromixer (HEM) will be modified (HEMsh) such that

$$W^* = \frac{W}{2} = 200\ \mu m$$

$$H = W * G$$

$$W_b = 80 \mu m$$

Where the parameters: *W, G, and* W_b are defined as in *Chapter V.1.1.* This leads to the considerations in *Table 20*.

Table 20: Modified Location Definitions

Name	HEM and SC	HEMsh
Location	Distance *L* (μm)	Distance *L* (μm)
C_1	780	480
C_2	1260	760
C_3	1740	1040
C_4	2220	1320
C_5	2700	1600
C_6	3180	1880

A comparison of each of the models is presented in *Figure 33* for clarity.

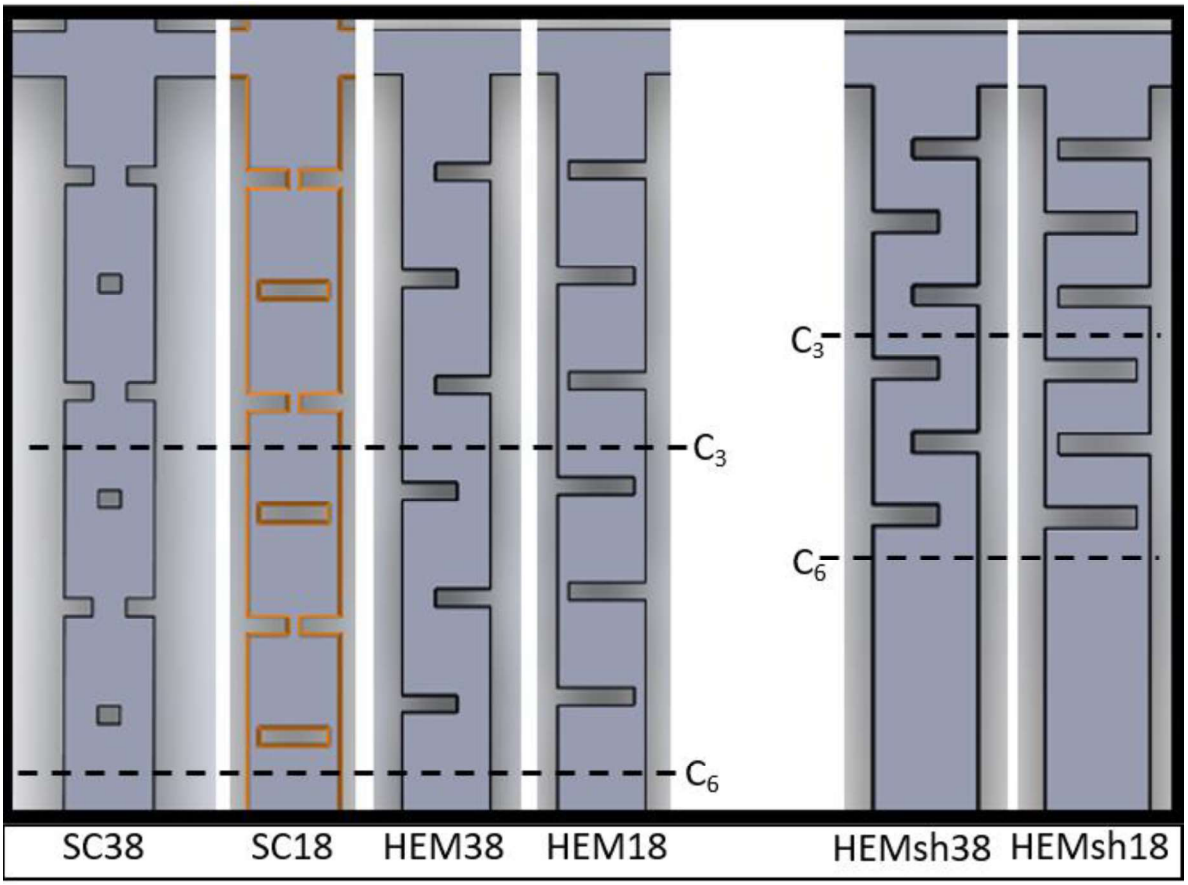

Figure 33: Comparing the SC, T, HEM, and HEMsh Models

Conducting the analysis for these models over the same range of input Reynolds and performing a comprehensive parameter analysis produces the results in *Figure 34*. Details of the plots can be found in *Appendix II*.

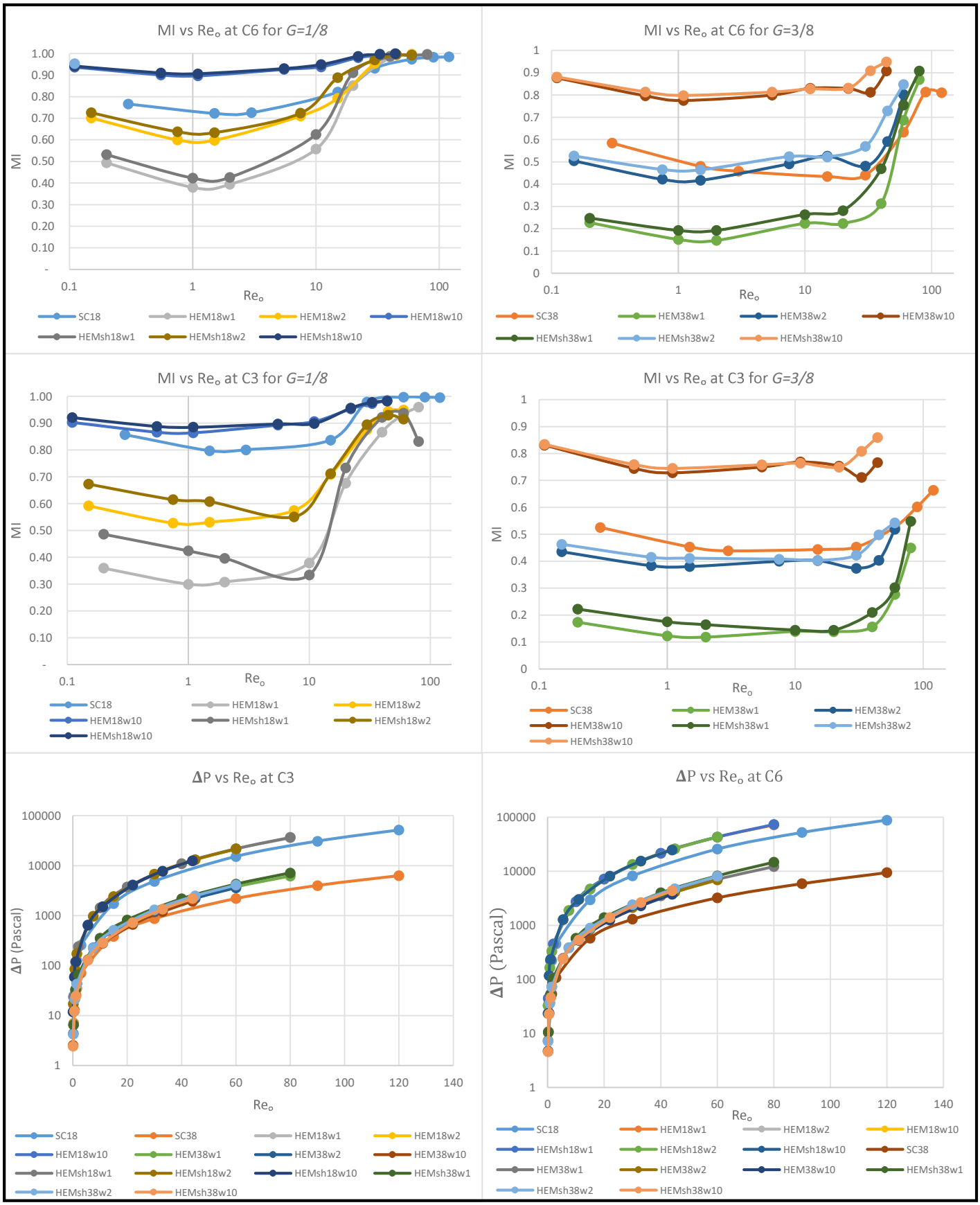

Figure 34:Results for the HEM Models

First, looking at the difference in *C3* and *C6* it is clear that the added length is likely not worth the marginal increase in efficiency, especially considering this gain is only practically significant in the *HEM* models. Additionally, looking at the difference in the full size and shortened models (*HEM* and *HEMsh,* respectively), the shorter model actually has greater efficiency for each case, though not significant. However, the fact that the efficiency *is* higher renders the longer model obsolete when trying to accomplish the design goal of having the shortest possible mixer. In considering the pressure differences across the different mixing units *C3* and *C6*, the pressure is less at *C3*, but only slightly suggesting that the majority of the losses occur at the junction itself. Additionally, as with the analysis of the *First Iteration Design*, the main contributor to pressure losses is the gap ratio at a specific outgoing Reynolds number rather than the flow weightings. It is important to note that the designed mixer does yield slightly higher losses for the same outgoing Reynolds number. However, in considering the mixing efficiencies obtained at a given pressure drop (*Figure 35*), the *HEMsh*18w10 model provides greatly improved mixing efficiencies for the entire range of Reynolds number for the same pressure drops, making this mixer much more practical. Additionally, a mixing index of 1 is achieved for a much lower pressure loss.

Comparing the mixing lengths and mixing efficiencies for each of the micromixers yields *Table 21* which presents results for an intermediate incoming Reynolds number of 20. This number is selected, because as presented in this thesis, lower Reynolds numbers benefit from diffusion and this falls in the specific range in which most micromixers operate.

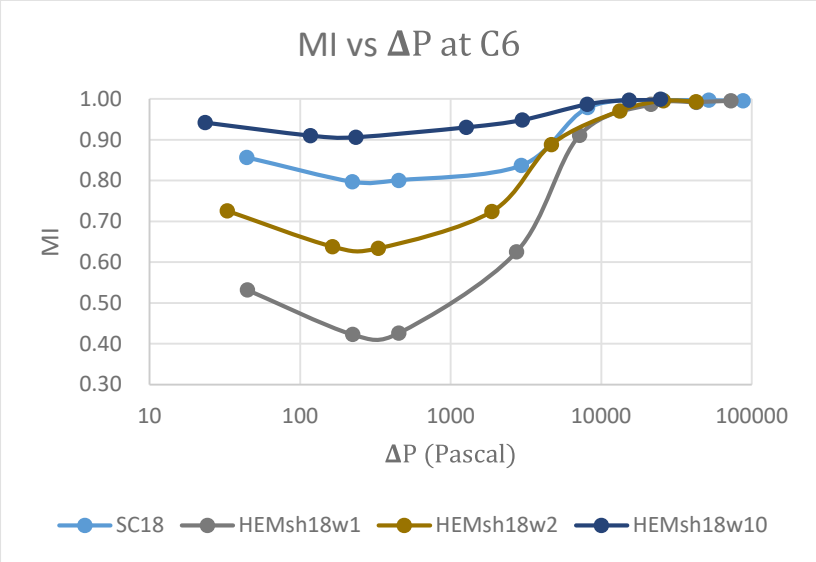

Figure 35: MI vs Pressure Drop comparison for HEMsh and SC

Table 21: Comparing Mixing Lengths and Indices for each Mixer

Mixer	Re_{in}	Re_o	Mixing Length (D_h)	MI
SC38	20	60	18.8	0.53
SC18	20	60	18.8	1.00
Tw1	20	40	34.45	0.18
Tw2	20	30	34.45	0.41
Tw10	20	22	34.45	0.61
HEMsh38w1	20	40	20.36	0.21
HEMsh38w2	20	30	20.36	0.42
HEMsh38w10	20	22	20.36	0.75
HEMsh18w1	20	40	11.27	0.92
HEMsh18w2	20	30	11.27	0.89
HEMsh18w10	20	22	11.27	0.96

There are a few important notes to be made about the results displayed here. First, in comparing the mixing index for the *T* series mixer that was designed, at higher w_f provides noticeable efficiency gains that can be achieved over the SC38 model, though the mixing lengths are longer. However, applying the work of the thesis in the development of the *HEMsh38* mixer yields appreciable gains over both the *T* series and *SC38* with comparable lengths to those in the *SC38*. Most notable is the *HEMsh18* mixer. This high efficiency mixer has efficiencies that are nearly identical to the *SC18* mixer while being 40 percent shorter. A comparison of the *HEMsh18w10* mixer to other mixers is presented in *Table 22.*

Table 22: Comparing the HEMsh model to other Mixers

Category	Type	Mixing Length (D_h)	MI	Reference
Lamination	Wedge Shaped Inlets	0.0667	0.9	[71]
Zig-Zag	Elliptic-shape Barriers	164	0.96	[72]
Embedded Barriers	Vortices	64	0.72	[73]
Twisted Channels	SAR	36	1	[74]
Surface	Obstacle Shape	10	0.98	[75]
Surface	T/Y mixer	10	0.95	[76]
SC18	Simple Planar Mixer	18.8	1.00	[7]
HEMsh18w110	Simpler Planar Mixer	11.27	0.96	------

In comparison to the other mixers presented above, the *HEMsh18*w110 is much simpler in design while providing higher efficiencies for much lower pressure and Reynolds operating conditions. Though the *HEMsh18w110* presents slightly less mixing efficiency, for a savings of

40 percent mixing length, and simpler design that reduces the number of inlets by one, the *HEMsh18w110* achieves the goal of micromixer design more completely.

Chapter V1: Conclusions and Discussion

This thesis established clear objectives to accomplish two main goals. The goals were 1) to determine a relationship between the entropy generation rate and the mixing efficiency and 2) develop a simple micromixer that achieved greater than 90 percent mixing efficiency for a wide range of Reynolds numbers. To achieve these goals, the thesis was guided by five intermediate objectives that independently constitute major conclusions of this thesis. The objectives and their conclusions are outlined followed by further discussion of each.

1. Determine a relationship between the mixing efficiency and the Reynolds number for several simple tee micromixers.

Chapter IV.1-IV.2 demonstrates the relative impact of the diffusive and chaotic advection on the mixing at set distances downstream within a simple *tee* micromixer leading to the development of a method to limit the observed mixing impact of diffusion to determine a linear analytical relationship between mixing efficiency and the outgoing Reynolds number.

2. Determine a relationship between the volumetric entropy generation rate and the Reynolds number for several simple tee micromixers.

Chapter IV.3 demonstrates a method for determining a correlation between the non-dimensionalized entropy generation rate that led to an analytical relationship between the entropy generation rate constituents and outgoing Reynolds numbers for a set of simple *tee* micromixers.

3. Determine a relationship between the mixing efficiency and the volumetric entropy generation rate for several simple tee micromixers.

   and

4. Develop relationships that hold for any scale.

Having developed independent analytical relationships for both mixing efficiency and entropy generation as a function of the same outgoing Reynolds number, a straightforward linear relationship is developed between the non-dimensionalized entropy generation rate constituents and the normalized mixing index demonstrating a clear linear relationship between these quantities.

5. Develop a simple micromixer that is an improvement on a current high efficiency micromixer.

In *Chapter V* the work relating to flow weightings as well as an investigation of another high efficiency micromixer, a new and simpler micromixer was designed that achieves greater than 90 percent efficiency for all of the target Reynolds numbers, with a 40 percent reduction in length when compared to its competitor.

A high performance micromixer is defined by achieving target mixing efficiencies quickly and in as compact a size as possible. Traditionally, these objectives are accomplished through very complex geometries that pose manufacturing challenges and introduce higher manufacturing costs. Additionally, micromixers are often developed to accomplish high mixing efficiencies for a single set of parameters. The problem with this approach is quickly evident when trying to repurpose a micromixer for even slight changes in flow parameters. To make any estimations on how the changes will affect the mixing efficiency, an entire analysis would need to be conducted. To address this issue, this thesis develops a method for determining simple analytical relationships that are devoid of scale, and are valid for any flow parameters within the micromixer. Though the results presented in this thesis are valid for only these sets of

micromixers and represent over 17,000 compute-core hours of simulations on a super-computing cluster, this process can be used for any arbitrary mixer. To further extend the work of the thesis, the findings are used to guide the development of a micromixer that is competitive with those that can be found in the current literature.

The first objective was to develop an analytical relationship between both the mixing efficiency and the entropy generation rate of the micromixer and the outgoing Reynolds number. For practical design purposes, all of the design constraints are known. Specifically, it is almost always known what flow rates can be achieved, and what the geometrical constraints are. Therefore, one can easily determine the Reynolds number that will be achieved in the mixer. With this parameter alone, one would simply need to calculate the mixing efficiency and entropy generation for the mixer (both quantities are important when analyzing micromixers). This analysis was conducted for a simple tee mixing geometry as a guide for more complex mixing geometries and to determine ways of easily increasing mixing efficiency through simply changing flow weighting at the entrances. The analytical relationships are presented as *Equations 43,46,* and *47*. An example calculation is conducted in *Appendix III*.

Second, an analytical relationship was determined for the mixing efficiency as a function of the entropy generation rate that is independent of scale. This thesis hypothesized a possible relationship between these two quantities, though prior to this thesis, to the author's knowledge, there have never been any analytical results of this kind developed. As this thesis presents, it would not be possible to develop a single analytical relationship that is non-dimensionalized and devoid of scale. However, when considering the separate constituents of entropy generation, simple analytical relationships can be developed for each of these constituents as function of the

mixing index. This is particularly useful, because it can be used to determine either mixing index or entropy generation rate when provided with the other.

Looking specifically at a major implication of the thesis, one could recognize the impact that increasing flow weightings has on the mixing efficiencies. For the simple tee utilized for the analysis, increased flow weighting directly contributes to sharp increases in mixing efficiency. Taking this result and applying it to the development of another micromixer, this thesis demonstrates a few things. First, through the *First Iteration Design* presented in *Chapter V.3*, for a flow weighting of 1 to 10, a low performance mixer (as described in *Chapter V.3*) can be significantly improved. Additionally, expanding the application in creating an HP mixer, through the use of flow weighting and obstacles a mixer was created that achieved greater than 90 percent mixing efficiency for a range of Reynolds 0.1 to 100 with pressure heads that are typically achievable in microscale devices for a broad range of flow rates. However, to further explore the practical applications of this mixer, a future analysis should be conducted for Reynolds less than 0.1 where some designs are constrained to such Reynolds numbers.

References

[1] Ahmed, D., Mao, X., Juluri, B. K., & Huang, T. J. (2009). A fast microfluidic mixer based on acoustically driven sidewall-trapped microbubbles. *Microfluidics and nanofluidics*, *7*(5), 727.

[2] Jeong, G. S., Chung, S., Kim, C. B., & Lee, S. H. (2010). Applications of micromixing technology. *Analyst*, *135*(3), 460-473.

[3] Hossain, S., Husain, A., & Kim, K. Y. (2011). Optimization of micromixer with staggered herringbone grooves on top and bottom walls. *Engineering Applications of Computational Fluid Mechanics*, *5*(4), 506-516.

[4] Shi, X., Xiang, Y., Wen, L. X., & Chen, J. F. (2012). CFD Analysis of flow patterns and micromixing efficiency in a Y-type microchannel reactor. *Industrial & Engineering Chemistry Research*, *51*(43), 13944-13952.

[5] Stroock, A. D., Dertinger, S. K., Ajdari, A., Mezić, I., Stone, H. A., & Whitesides, G. M. (2002). Chaotic mixer for microchannels. *Science*, *295*(5555), 647-651.

[6] Yang, J. T., Huang, K. J., & Lin, Y. C. (2005). Geometric effects on fluid mixing in passive grooved micromixers. *Lab on a Chip*, *5*(10), 1140-1147.

[7] Shih, T. R., & Chung, C. K. (2008). A high-efficiency planar micromixer with convection and diffusion mixing over a wide Reynolds number range. *Microfluidics and Nanofluidics*, *5*(2), 175-183.

[8] Lu, L. H., Ryu, K. S., & Liu, C. (2002). A magnetic microstirrer and array for microfluidic mixing. *Journal of microelectromechanical systems*, *11*(5), 462-469.

[9] Muradoglu, M., & Stone, H. A. (2005). Mixing in a drop moving through a serpentine channel: a computational study. *Physics of Fluids (1994-present)*, *17*(7), 073305.

[10] Devahastin, S., & Mujumdar, A. S. (2002). A numerical study of flow and mixing characteristics of laminar confined impinging streams. *Chemical Engineering Journal*, *85*(2), 215-223.

[11] Wang, S. J., Devahastin, S., & Mujumdar, A. S. (2005). A numerical investigation of some approaches to improve mixing in laminar confined impinging streams. *Applied thermal engineering*, *25*(2), 253-269.

[12] Song, H., Bringer, M. R., Tice, J. D., Gerdts, C. J., & Ismagilov, R. F. (2003). Experimental test of scaling of mixing by chaotic advection in droplets moving through microfluidic channels. *Applied Physics Letters*, *83*(22), 4664-4666.

[13] Soleymani, A., Kolehmainen, E., & Turunen, I. (2008). Analytical and experimental investigations of liquid mixing in T-type micromixers. *Chemical engineering journal*, *135*, S219-S228.

[14] Mengeaud, V., Josserand, J., & Girault, H. H. (2002). Mixing processes in a zigzag microchannel: finite element simulations and optical study. *Analytical chemistry*, *74*(16), 4279-4286.

[15] Campisi, M., Accoto, D., Damiani, F., & Dario, P. (2009). A soft-lithographed chaotic electrokinetic micromixer for efficient chemical reactions in lab-on-chips. Journal of Micro-Nano Mechatronics, 5(3-4), 69-76.

[16] Cho, C. C. (2008). Electrokinetically driven flow mixing utilizing chaotic electric fields. *Microfluidics and nanofluidics*, *5*(6), 785-793.

[17] Du, Y., Zhang, Z., Yim, C., Lin, M., & Cao, X. (2010). A simplified design of the staggered herringbone micromixer for practical applications. *Biomicrofluidics*, *4*(2), 024105.

[18] Wang, Y., Zhe, J., Chung, B. T., & Dutta, P. (2008). A rapid magnetic particle driven micromixer. *Microfluidics and Nanofluidics*, *4*(5), 375-389.

[19] Niu, X., & Lee, Y. K. (2003). Efficient spatial-temporal chaotic mixing in microchannels. *Journal of Micromechanics and Microengineering*, *13*(3), 454.

[20] Xu, B., Wong, T. N., Nguyen, N. T., Che, Z., & Chai, J. C. K. (2010). Thermal mixing of two miscible fluids in a T-shaped microchannel. *Biomicrofluidics*, *4*(4), 044102.

[21] Nguyen, N. T., & Wu, Z. (2004). Micromixers—a review. *Journal of Micromechanics and Microengineering*, *15*(2), R1.

[22] Saffaripour, M., & Culham, R. (2010). Measurement of Entropy Generation in Microscale Thermal-Fluid Systems. *Journal of Heat Transfer*, *132*(12), 121401.

[23] Luong, T. D., Phan, V. N., & Nguyen, N. T. (2011). High-throughput micromixers based on acoustic streaming induced by surface acoustic wave. *Microfluidics and nanofluidics*, *10*(3), 619-625.

[24] Lim, C. Y., Lam, Y. C., & Yang, C. (2010). Mixing enhancement in microfluidic channel with a constriction under periodic electro-osmotic flow. *Biomicrofluidics*, *4*(1), 014101.

[25] Zhang, Z., Yim, C., Lin, M., & Cao, X. (2008). Quantitative characterization of micromixing simulation. *Biomicrofluidics*, *2*(3), 034104.

[26] Lam, Y. C., Gan, H. Y., Nguyen, N. T., & Lie, H. (2009). Micromixer based on viscoelastic flow instability at low Reynolds number. *Biomicrofluidics*, *3*(1), 014106.

[27] Liu, R. H., Stremler, M. A., Sharp, K. V., Olsen, M. G., Santiago, J. G., Adrian, R. J., ... & Beebe, D. J. (2000). Passive mixing in a three-dimensional serpentine microchannel. Journal of microelectromechanical systems, 9(2), 190-197.

[28] Vijayendran, R. A., Motsegood, K. M., Beebe, D. J., & Leckband, D. E. (2003). Evaluation of a three-dimensional micromixer in a surface-based biosensor. Langmuir, 19(5), 1824-1828.

[29] Chen, H., & Meiners, J. C. (2004). Topologic mixing on a microfluidic chip. Applied Physics Letters, 84(12), 2193-2195.

[30] Park, S. J., Kim, J. K., Park, J., Chung, S., Chung, C., & Chang, J. K. (2003). Rapid three-dimensional passive rotation micromixer using the breakup process. Journal of Micromechanics and Microengineering, 14(1), 6.

[31] Jen, C. P., Wu, C. Y., Lin, Y. C., & Wu, C. Y. (2003). Design and simulation of the micromixer with chaotic advection in twisted microchannels. Lab on a Chip, 3(2), 77-81.

[32] Evans, J., Liepmann, D., & Pisano, A. P. (1997, January). Planar laminar mixer. In Proc. IEEE MEMS Workshop (Vol. 10, pp. 96-101).

[33] Johnson, T. J., Ross, D., & Locascio, L. E. (2002). Rapid microfluidic mixing. Analytical chemistry, 74(1), 45-51.

[34] Stroock, A. D., & Whitesides, G. M. (2003). Controlling flows in microchannels with patterned surface charge and topography. Accounts of chemical research, 36(8), 597-604.

[35] Wang, H., Iovenitti, P., Harvey, E., & Masood, S. (2003). Analytical investigation of mixing in microchannels with patterned grooves. Journal of Micromechanics and Microengineering, 13(6), 801.

[36] Biddiss, E., Erickson, D., & Li, D. (2004). Heterogeneous surface charge enhanced micromixing for electrokinetic flows. Analytical Chemistry, 76(11), 3208-3213.

[37] Kim, D. S., Lee, S. W., Kwon, T. H., & Lee, S. S. (2004). A barrier embedded chaotic micromixer. Journal of micromechanics and microengineering, 14(6), 798.

[38] Wang, H., Iovenitti, P., Harvey, E., & Masood, S. (2002). Optimizing layout of obstacles for enhanced mixing in microchannels. Smart materials and structures, 11(5), 662.

[39] Lin, Y., Gerfen, G. J., Rousseau, D. L., & Yeh, S. R. (2003). Ultrafast microfluidic mixer and freeze-quenching device. Analytical chemistry, 75(20), 5381-5386.

[40] Hong, C. C., Choi, J. W., & Ahn, C. H. (2004). A novel in-plane passive microfluidic mixer with modified Tesla structures. Lab on a Chip, 4(2), 109-113.

[41] Huang, M. Z., Yang, R. J., Tai, C. H., Tsai, C. H., & Fu, L. M. (2006). Application of electrokinetic instability flow for enhanced micromixing in cross-shaped microchannel. *Biomedical microdevices*, *8*(4), 309-315.

[42] Oztop, H. F., & Al-Salem, K. (2012). A review on entropy generation in natural and mixed convection heat transfer for energy systems. *Renewable and Sustainable Energy Reviews*, *16*(1), 911-920.

[43] Kamholz, A. E., Weigl, B. H., Finlayson, B. A., & Yager, P. (1999). Quantitative analysis of molecular interaction in a microfluidic channel: the T-sensor. Analytical chemistry, 71(23), 5340-5347.

[44] Kamholz, A. E., & Yager, P. (2002). Molecular diffusive scaling laws in pressure-driven microfluidic channels: deviation from one-dimensional Einstein approximations. Sensors and Actuators B: Chemical, 82(1), 117-121.

[45] Wong, S. H., Ward, M. C., & Wharton, C. W. (2004). Micro T-mixer as a rapid mixing micromixer. Sensors and Actuators B: Chemical, 100(3), 359-379.

[46] Gobby, D., Angeli, P., & Gavriilidis, A. (2001). Mixing characteristics of T-type microfluidic mixers. Journal of Micromechanics and microengineering, 11(2), 126.

[47] Veenstra, T. T., Lammerink, T. S. J., Elwenspoek, M. C., & Van Den Berg, A. (1999). Characterization method for a new diffusion mixer applicable in micro flow injection analysis systems. Journal of Micromechanics and Microengineering, 9(2), 199.

[48] Hadd, A. G., Raymond, D. E., Halliwell, J. W., Jacobson, S. C., & Ramsey, J. M. (1997). Microchip device for performing enzyme assays. Analytical Chemistry, 69(17), 3407-3412.

[49] Ismagilov, R. F., Stroock, A. D., Kenis, P. J., Whitesides, G., & Stone, H. A. (2000). Experimental and theoretical scaling laws for transverse diffusive broadening in two-phase laminar flows in microchannels. Applied Physics Letters, 76(17), 2376-2378.

[50] Hinsmann, P., Frank, J., Svasek, P., Harasek, M., & Lendl, B. (2001). Design, simulation and application of a new micromixing device for time resolved infrared spectroscopy of chemical reactions in solution. Lab on a Chip, 1(1), 16-21.

[51] Wu, Z., Nguyen, N. T., & Huang, X. (2004). Nonlinear diffusive mixing in microchannels: theory and experiments. Journal of Micromechanics and Microengineering, 14(4), 604.

[52] Yi, M., & Bau, H. H. (2003). The kinematics of bend-induced mixing in micro-conduits. International Journal of Heat and Fluid Flow, 24(5), 645-656.

[53] Böhm, S., Greiner, K., Schlautmann, S., de Vries, S., & van den Berg, A. (2001). A rapid vortex micromixer for studying high-speed chemical reactions. In Micro Total Analysis Systems 2001 (pp. 25-27). Springer Netherlands.

[54] Wong, S. H., Bryant, P., Ward, M., & Wharton, C. (2003). Investigation of mixing in a cross-shaped micromixer with static mixing elements for reaction kinetics studies. Sensors and Actuators B: Chemical, 95(1), 414-424.

[55] Koch, M., Witt, H., Evans, A. G. R., & Brunnschweiler, A. (1999). Improved characterization technique for micromixers. Journal of Micromechanics and Microengineering, 9(2), 156.

[56] Bessoth, F. G., & Manz, A. (1999). Microstructure for efficient continuous flow mixing. Analytical communications, 36(6), 213-215.

[57] Knight, J. B., Vishwanath, A., Brody, J. P., & Austin, R. H. (1998). Hydrodynamic focusing on a silicon chip: mixing nanoliters in microseconds. Physical Review Letters, 80(17), 3863.

[58] Walker, G. M., Ozers, M. S., & Beebe, D. J. (2004). Cell infection within a microfluidic device using virus gradients. Sensors and Actuators B: Chemical, 98(2), 347-355.

[59] Branebjerg, J., Gravesen, P., Krog, J. P., & Nielsen, C. R. (1996, February). Fast mixing by lamination. In Micro Electro Mechanical Systems, 1996, MEMS'96, Proceedings. An Investigation of Micro Structures, Sensors, Actuators, Machines and Systems. IEEE, The Ninth Annual International Workshop on (pp. 441-446). IEEE.

[60] Schwesinger, N., Frank, T., & Wurmus, H. (1996). A modular microfluid system with an integrated micromixer. Journal of Micromechanics and Microengineering, 6(1), 99.

[61] Gray, B. L., Jaeggi, D., Mourlas, N. J., Van Drieenhuizen, B. P., Williams, K. R., Maluf, N. I., & Kovacs, G. T. A. (1999). Novel interconnection technologies for integrated microfluidic systems. Sensors and Actuators A: Physical, 77(1), 57-65.

[62] Munson, M. S., & Yager, P. (2004). Simple quantitative optical method for monitoring the extent of mixing applied to a novel microfluidic mixer. Analytica Chimica Acta, 507(1), 63-71.

[63] He, B., Burke, B. J., Zhang, X., Zhang, R., & Regnier, F. E. (2001). A picoliter-volume mixer for microfluidic analytical systems. Analytical Chemistry, 73(9), 1942-1947.

[64] Melin, J., Giménez, G., Roxhed, N., van der Wijngaart, W., & Stemme, G. (2004). A fast passive and planar liquid sample micromixer. Lab on a Chip, 4(3), 214-219.

[65] Miyake, R., Lammerink, T. S., Elwenspoek, M., & Fluitman, J. H. (1993, February). Micro mixer with fast diffusion. In Micro Electro Mechanical Systems, 1993, MEMS'93, Proceedings An Investigation of Micro Structures, Sensors, Actuators, Machines and Systems. IEEE. (pp. 248-253). IEEE.

[66] Miyake, R., Tsuzuki, K., Takagi, T., & Imai, K. (1997). A highly sensitive and small flow-type chemical analysis system with integrated absorptiometric micro-flowcell. IEEJ Transactions on Sensors and Micromachines, 117(3), 147-154.

[67] Larsen, U. D., Rong, W., & Telleman, P. (1999, June). Design of rapid micromixers using CFD. In Proc. Transducers' 99, 10th Int. Conf. on Solid-State Sensors and Actuators (Sendai, Japan) (pp. 200-3).

[68] Seidel, R. U., Si, D. Y., Menz, W., & Esashi, M. (1999). Capillary force mixing device as sampling module for chemical analysis. In Proc. Transducers' 99, 10th Int. Conf. on Solid-State Sensors and Actuators (Sendai, Japan) (pp. 438-41).

[69] Voldman, J., Gray, M. L., & Schmidt, M. A. (2000). An integrated liquid mixer/valve. Journal of Microelectromechanical Systems, 9(3), 295-302.

[70] Hessel, V., Löwe, H., & Schönfeld, F. (2005). Micromixers—a review on passive and active mixing principles. *Chemical Engineering Science*, *60*(8), 2479-2501.

[71] Buchegger, W., Wagner, C., Lendl, B., Kraft, M., & Vellekoop, M. J. (2011). A highly uniform lamination micromixer with wedge shaped inlet channels for time resolved infrared spectroscopy. Microfluidics and Nanofluidics, 10(4), 889-897.

[72] Lee, C. Y., Lin, C., Hung, M. F., Ma, R. H., Tsai, C. H., Lin, C. H., & Fu, L. M. (2006). Experimental and analytical investigation into mixing efficiency of micromixers with different geometric barriers. In Materials science forum (Vol. 505, pp. 391-396). Trans Tech Publications.

[73] Tsai, R. T., & Wu, C. Y. (2011). An efficient micromixer based on multidirectional vortices due to baffles and channel curvature. Biomicrofluidics, 5(1), 014103.

[74] Hardt, S., Pennemann, H., & Schönfeld, F. (2006). Theoretical and experimental characterization of a low-Reynolds number split-and-recombine mixer. Microfluidics and Nanofluidics, 2(3), 237-248.

[75] Jain, M., Yeung, A., & Nandakumar, K. (2009). Induced charge electro osmotic mixer: Obstacle shape optimization. Biomicrofluidics, 3(2), 022413.

[76] Jain, M., & Nandakumar, K. (2010). Novel index for micromixing characterization and comparative analysis. Biomicrofluidics, 4(3), 031101.

[77] Lee, C. Y., Chang, C. L., Wang, Y. N., & Fu, L. M. (2011). Microfluidic mixing: a review. *International journal of molecular sciences*, *12*(5), 3263-3287.

[78] Viktorov, V., Mahmud, M. R., & Visconte, C. (2016). Analytical study of fluid mixing at different inlet flow-rate ratios in Tear-drop and Chain micromixers compared to a new HC passive micromixer. *Engineering Applications of Computational Fluid Mechanics*, *10*(1), 183-193.

[79] Kawabe, T., Hayamizu, Y., Yanase, S., Gonda, T., Morita, S., Ohtsuka, S., & Yamamoto, K. (2014). A Micromixer Using the Taylor-Dean Flow: Effect of Inflow Conditions on the Mixing. *Open Journal of Fluid Dynamics*, *4*(05), 463.

[80] Hayamizu, Y., Kawabe, T., Yanase, S., Gonda, T., Morita, S., Ohtsuka, S., & Yamamoto, K. (2015). A Micromixer Using the Taylor-Dean Flow: Effects of Aspect Ratio and Inflow Condition on the Mixing. *Open Journal of Fluid Dynamics*, *5*(03), 256.

[81] Mizuno, Y., & Funakoshi, M. (2002). Chaotic mixing due to a spatially periodic three-dimensional flow. Fluid dynamics research, 31(2), 129-149.

[82] Lim, D., Kamotani, Y., Cho, B., Mazumder, J., & Takayama, S. (2003). Fabrication of microfluidic mixers and artificial vasculatures using a high-brightness diode-pumped Nd: YAG laser direct write method. Lab on a Chip, 3(4), 318-323.

[83] Hau, W. L., Trau, D. W., Sucher, N. J., Wong, M., & Zohar, Y. (2003). Surface-chemistry technology for microfluidics. Journal of micromechanics and microengineering, 13(2), 272.

[84] Jones, S. W., & Aref, H. (1988). Chaotic advection in pulsed source–sink systems. The Physics of fluids, 31(3), 469-485.

[85] Tofteberg, T., Skolimowski, M., Andreassen, E., & Geschke, O. (2010). A novel passive micromixer: lamination in a planar channel system. Microfluidics and Nanofluidics, 8(2), 209-215.

[86] Chen, Z., Bown, M. R., O'Sullivan, B., MacInnes, J. M., Allen, R. W. K., Mulder, M., ... & van't Oever, R. (2009). Performance analysis of a folding flow micromixer. Microfluidics and nanofluidics, 6(6), 763-774.

[87] Kang, T. G., Singh, M. K., Anderson, P. D., & Meijer, H. E. (2009). A chaotic serpentine mixer efficient in the creeping flow regime: from design concept to optimization. Microfluidics and nanofluidics, 7(6), 783.

[88] Moon, D., & Migler, K. B. (2010). Forced assembly and mixing of melts via planar polymer Neerincx, P. E., Denteneer, R. P., Peelen, S., & Meijer, H. E. (2011). Compact mixing using multiple splitting, stretching, and recombining flows. Macromolecular Materials and Engineering, 296(3-4), 349-361. micro-mixing. Polymer, 51(14), 3147-3155.

[89] Lin, C. H., Tsai, C. H., & Fu, L. M. (2005). A rapid three-dimensional vortex micromixer utilizing self-rotation effects under low Reynolds number conditions. Journal of Micromechanics and Microengineering, 15(5), 935.

[90] Singh, M. K., Anderson, P. D., & Meijer, H. E. (2009). Understanding and optimizing the SMX static mixer. Macromolecular rapid communications, 30(4-5), 362-376.

[91] Gregg, M. C. (1984). Entropy generation in the ocean by small-scale mixing. *Journal of physical oceanography*, *14*(4), 688-711.

[92] McEligot, D. M., Walsh, E. J., Laurien, E., & Spalart, P. R. (2008). Entropy generation in the viscous parts of turbulent boundary layers. *Journal of Fluids Engineering*, *130*(6), 061205.

[93] Bejan, A. (1996). Entropy generation minimization: The new thermodynamics of finite-size devices and finite-time processes. *Journal of Applied Physics*, *79*(3), 1191-1218.

[94] Magherbi, M., Abbassi, H., Hidouri, N., & Brahim, A. B. (2006). Second law analysis in convective heat and mass transfer. *Entropy*, *8*(1), 1-17.

[95] Sanchez, M., Henderson, A. W., Papavassiliou, D. V., & Lemley, E. C. (2012, July). Entropy Generation in Laminar Flow Junctions. In *ASME 2012 Fluids Engineering Division Summer Meeting collocated with the ASME 2012 Heat Transfer Summer Conference and the ASME 2012 10th International Conference on Nanochannels, Microchannels, and Minichannels* (pp. 325-330). American Society of Mechanical Engineers.

[96] Del Giudice, S., Nonino, C., & Savino, S. (2007). Effects of viscous dissipation and temperature dependent viscosity in thermally and simultaneously developing laminar flows in microchannels. *International journal of heat and fluid flow*, *28*(1), 15-27.

[97] Koo, J., & Kleinstreuer, C. (2004). Viscous dissipation effects in microtubes and microchannels. *International Journal of Heat and Mass Transfer*, *47*(14), 3159-3169.

[98] Schmandt, B., & Herwig, H. (2011). Loss coefficients in laminar flows: essential for the design of micro flow systems. *PAMM*, *11*(1), 27-30.

[99] Schmandt, B., & Herwig, H. (2011). Internal flow losses: A fresh look at old concepts. *Journal of Fluids Engineering*, *133*(5), 051201.

[100] Schmandt, B., & Herwig, H. (2011). Diffuser and nozzle design optimization by entropy generation minimization. *Entropy*, *13*(7), 1380-1402.

[101] Fargie, D., & Martin, B. W. (1971, March). Developing laminar flow in a pipe of circular cross-section. In *Proceedings of the Royal Society of London A: Mathematical, Physical and Engineering Sciences* (Vol. 321, No. 1547, pp. 461-476). The Royal Society.

[102] Niavarani, A., & Priezjev, N. V. (2009). The effective slip length and vortex formation in laminar flow over a rough surface. *Physics of Fluids (1994-present)*, *21*(5), 052105.

[103] Wilke, C. R., & Chang, P. (1955). Correlation of diffusion coefficients in dilute solutions. *AIChE Journal*, *1*(2), 264-270.

Appendix I: Chapter IV Plots

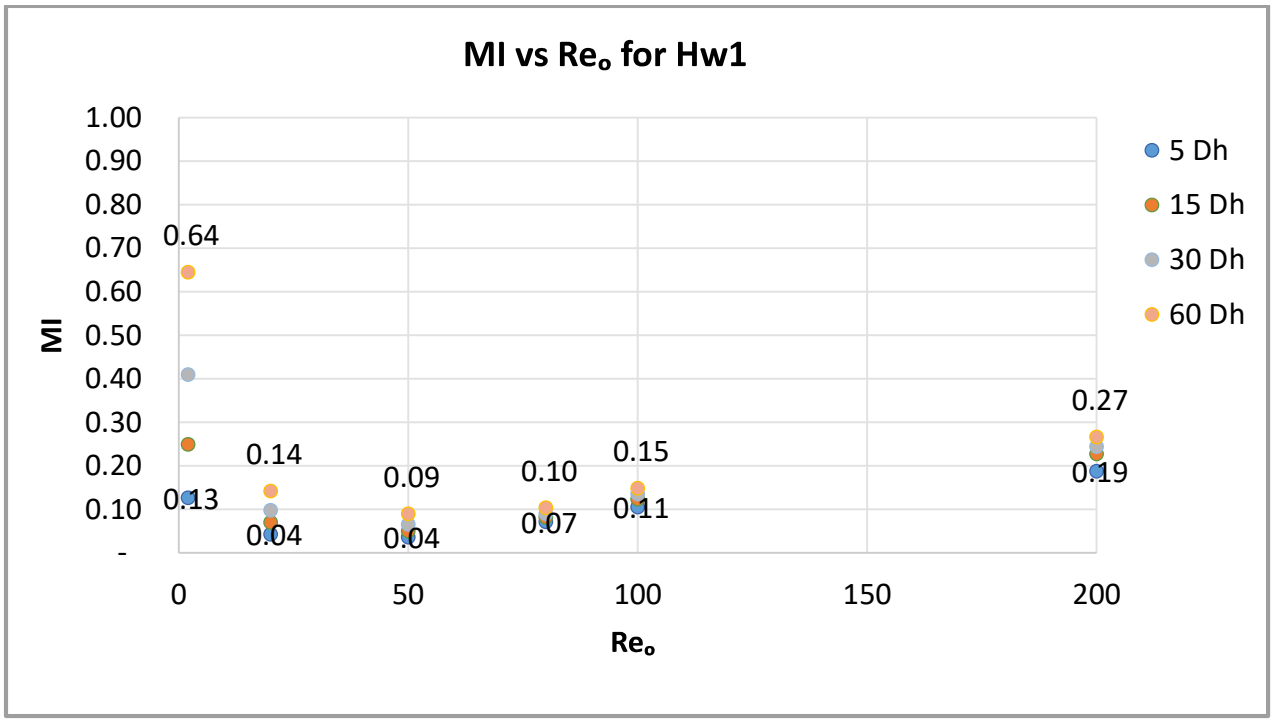

Figure 36: Detail of Hw1 MI

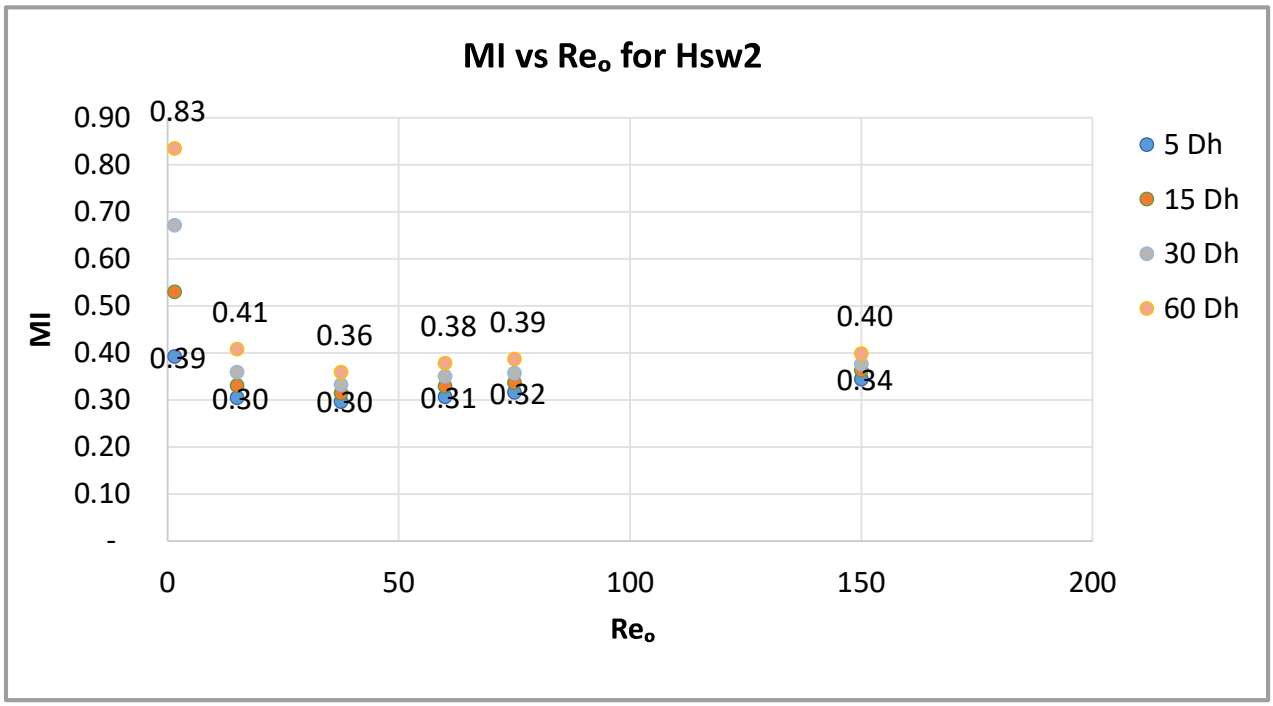

Figure 37: Details of Hsw2 MI

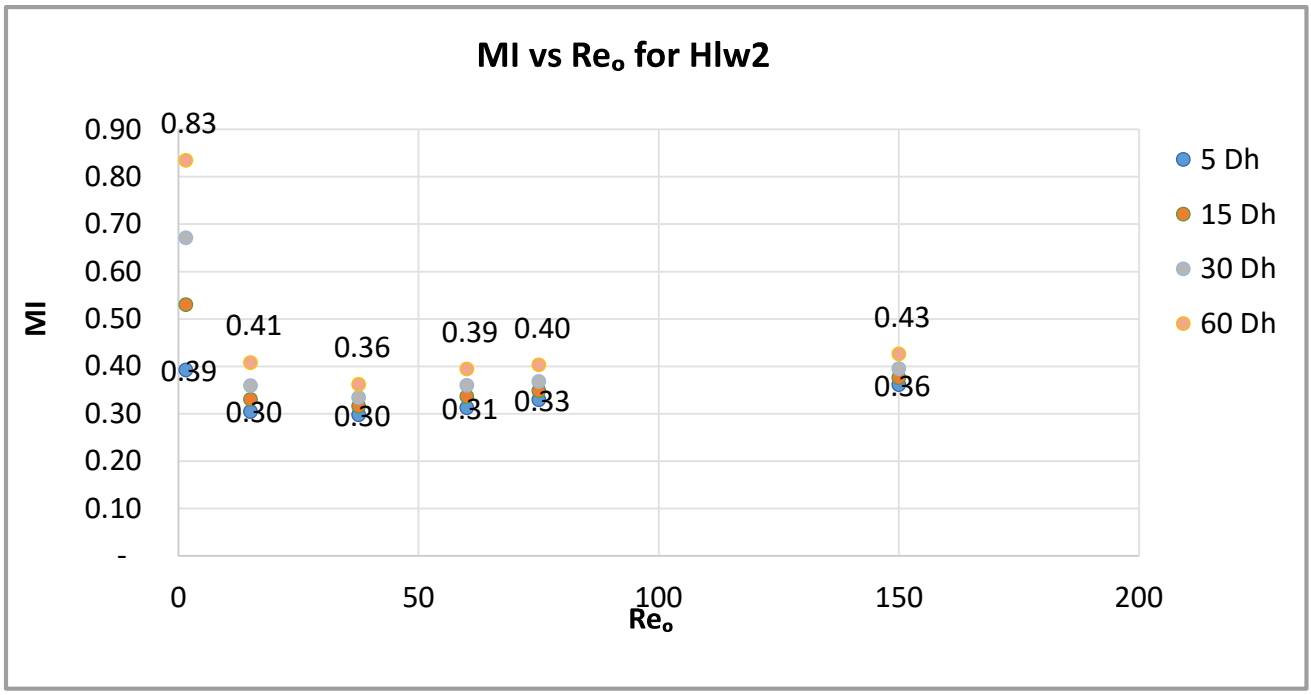

Figure 38: Details of Hlw2 MI

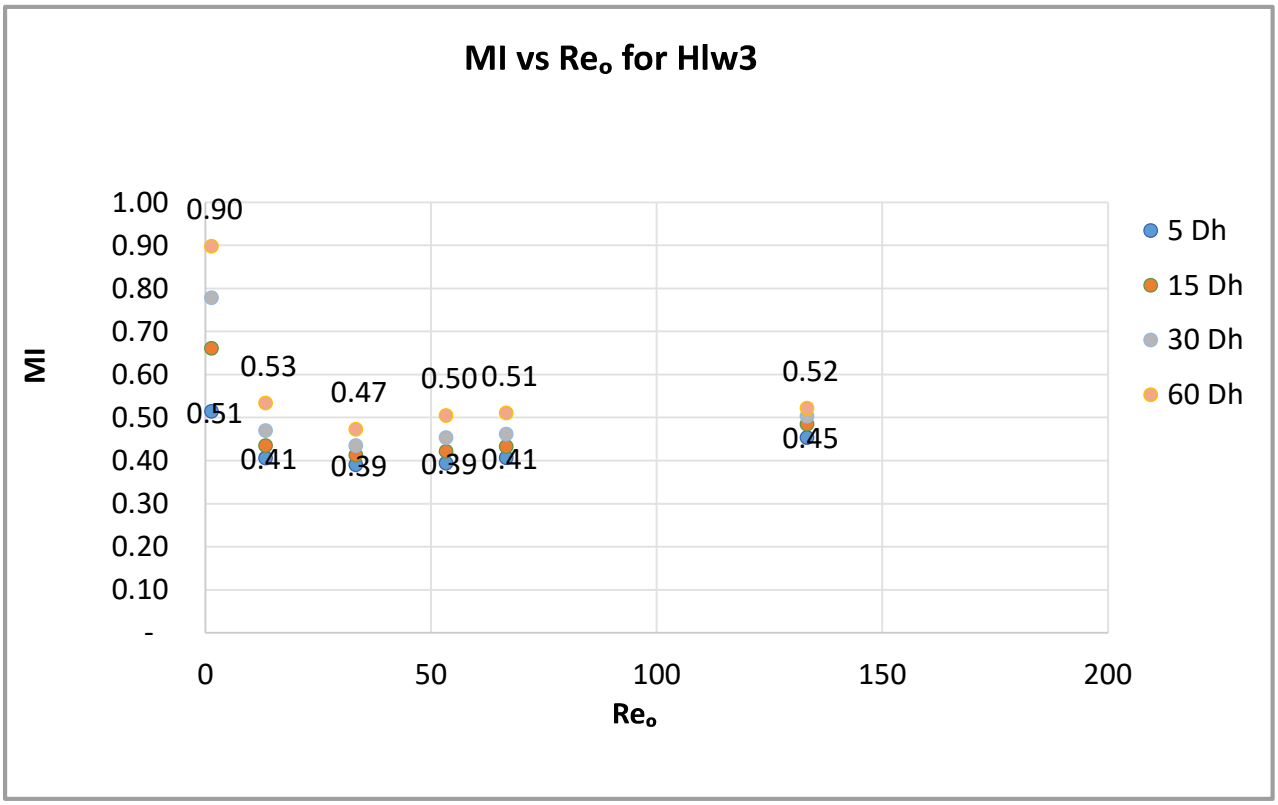

Figure 39: Details of Hlw3 MI

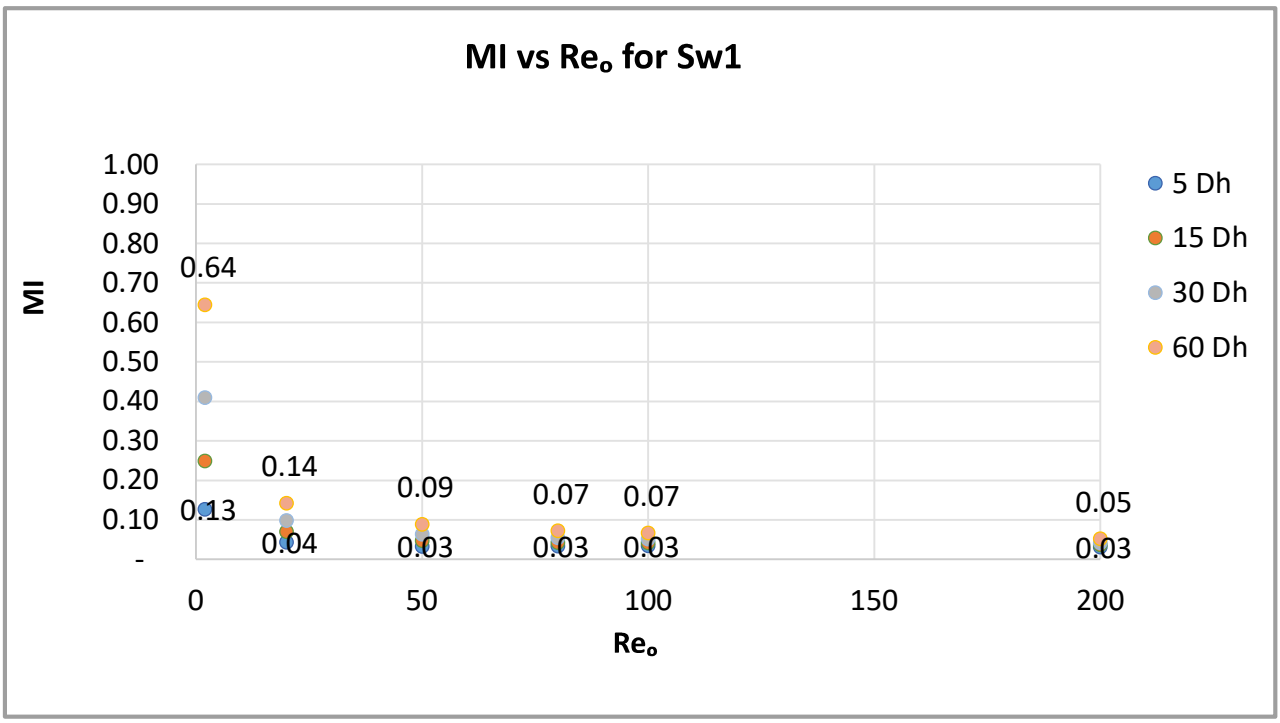

Figure 40: Details of Sw1 MI

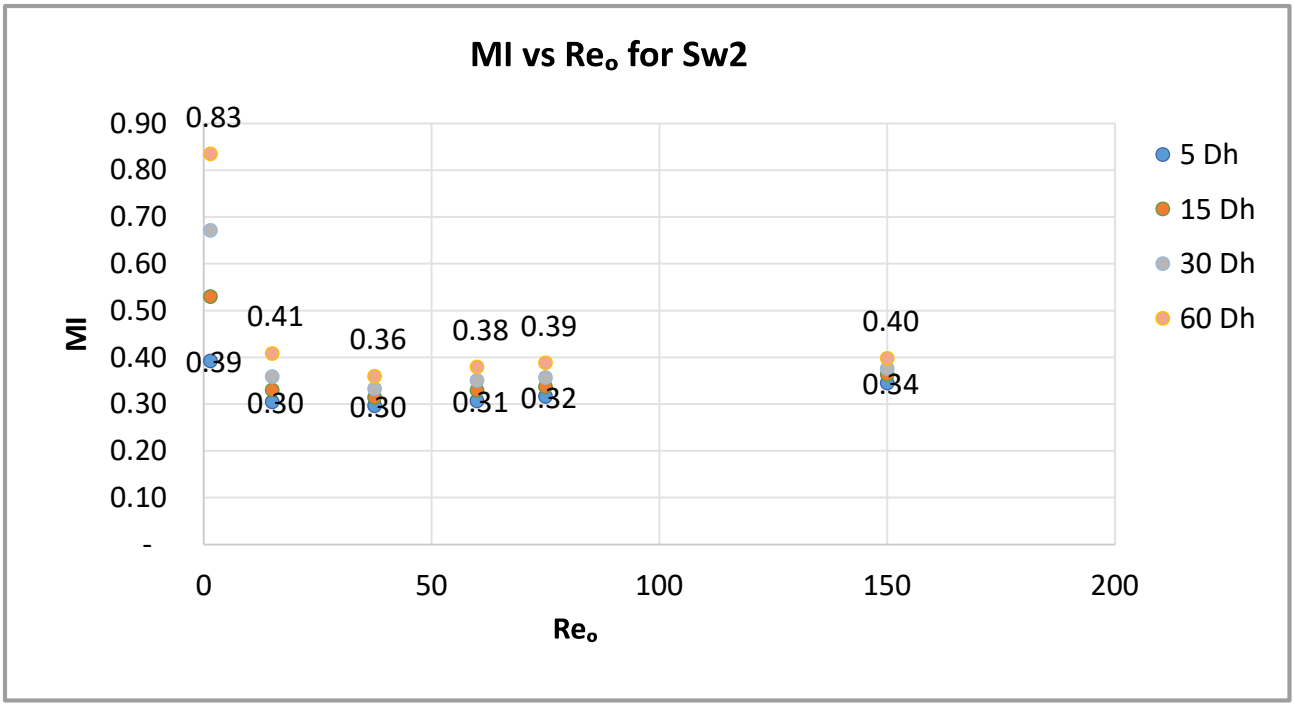

Figure 41: Details of Sw2 MI

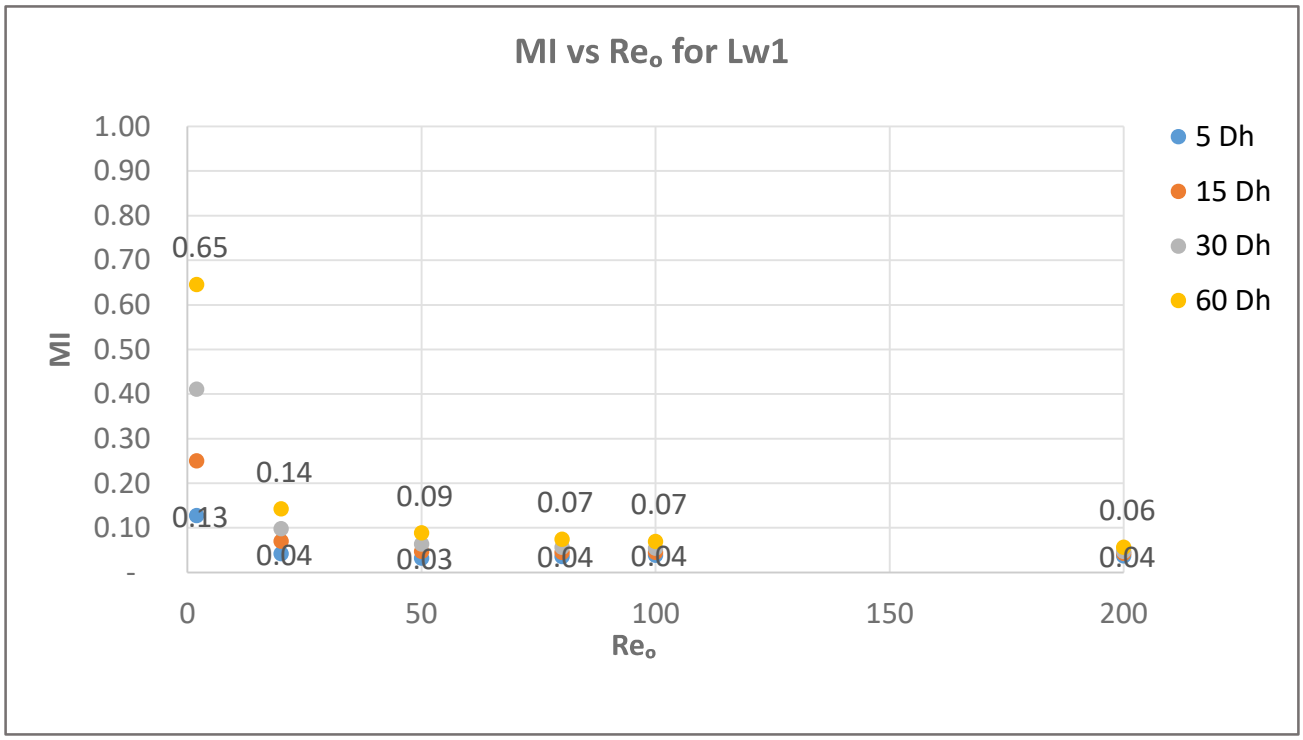

Figure 42: Details of Lw1 MI

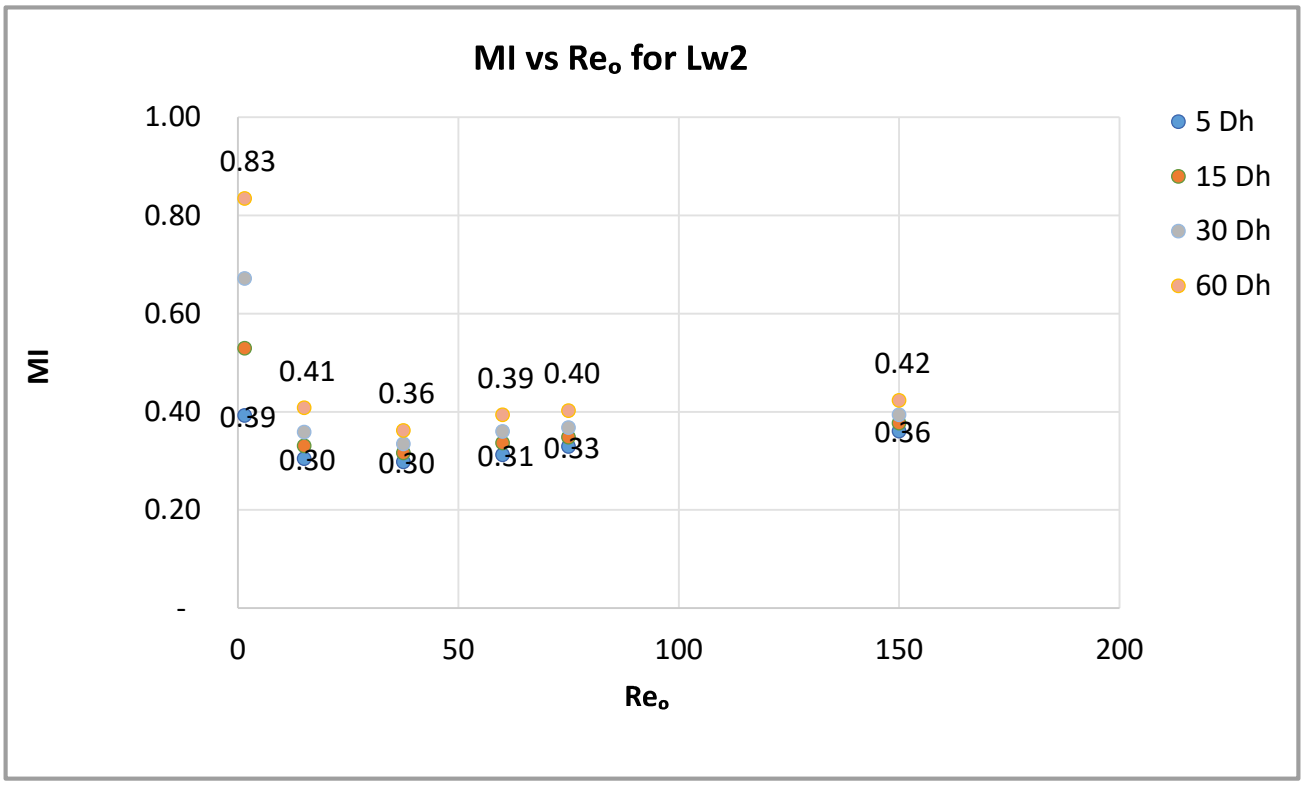

Figure 43: Details of Lw2 MI

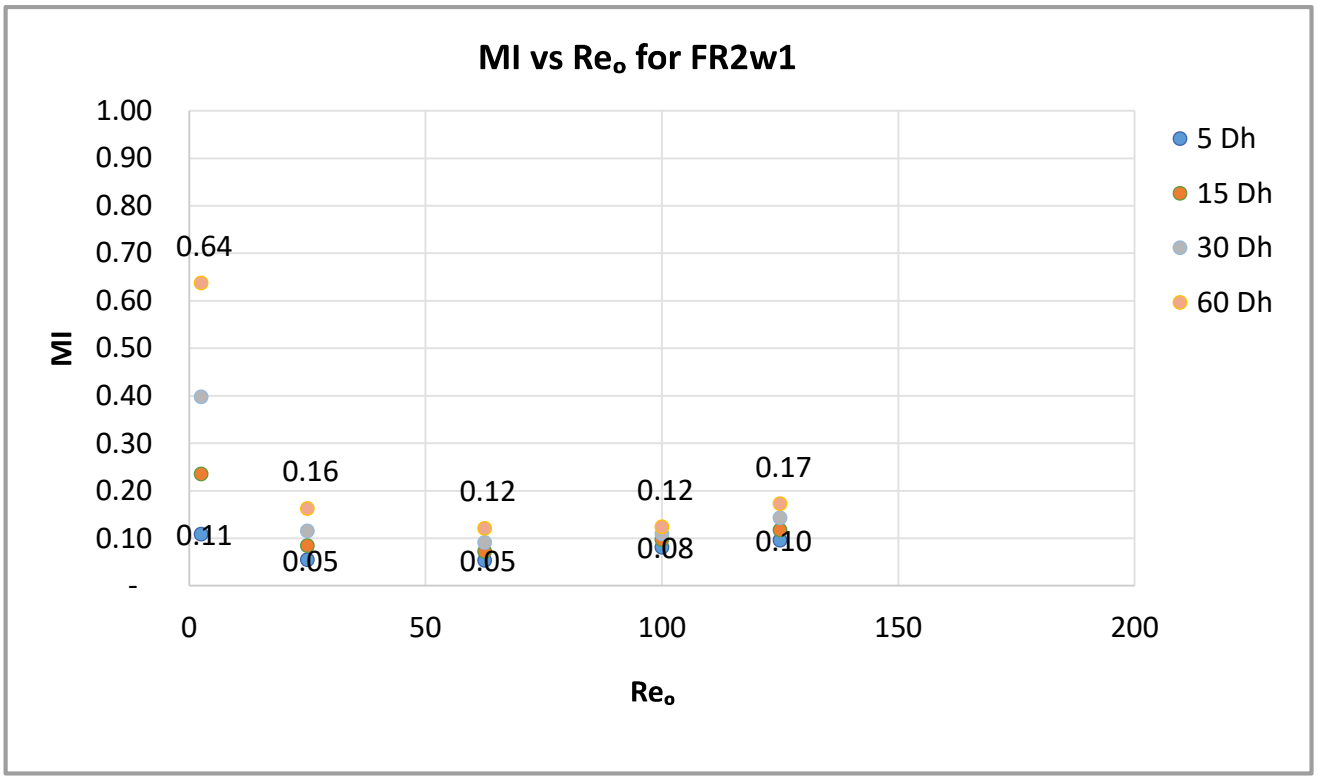

Figure 44: Details of FR2w1 MI

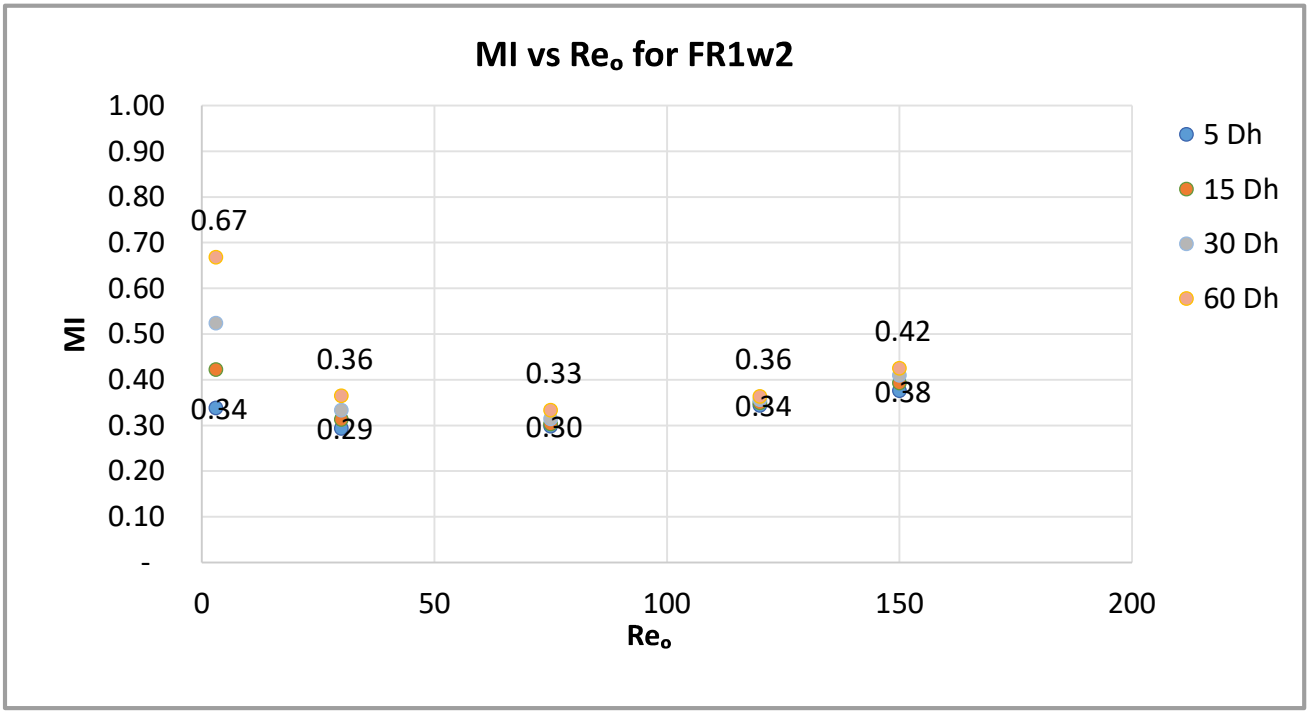

Figure 45: Details of FR1w2 MI

Appendix II: Chapter V Plots

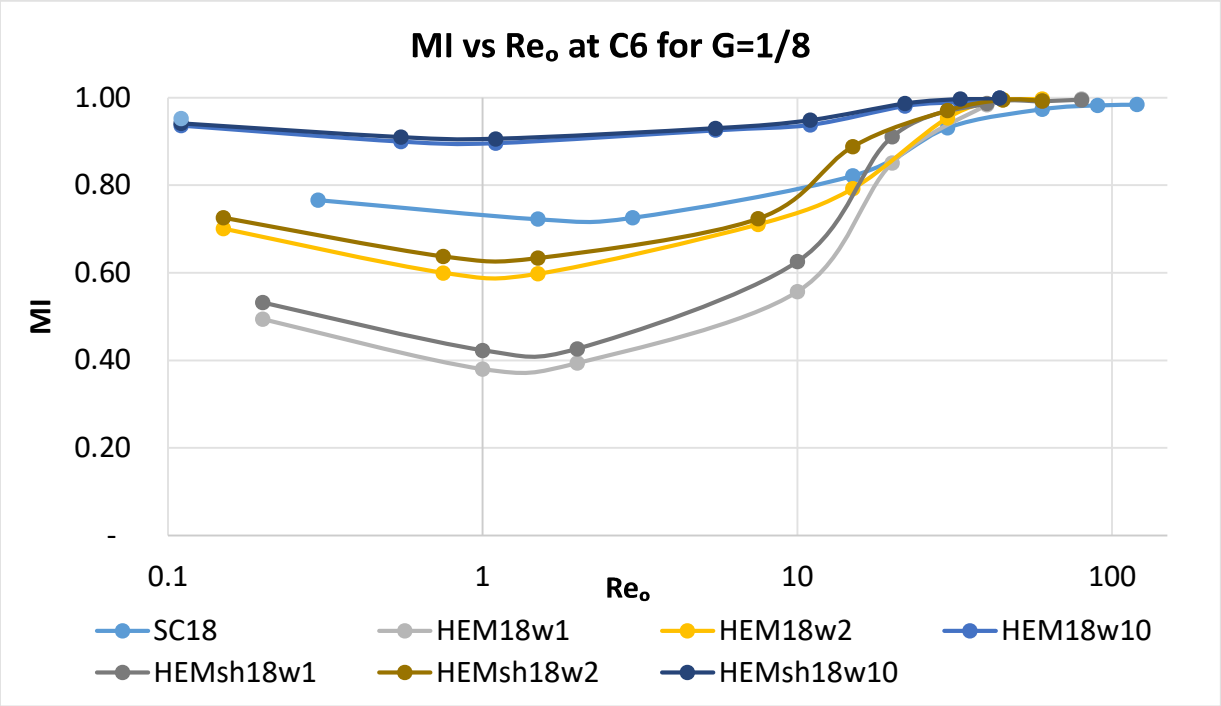

Figure 46: Details of G=1/8, C6 MI

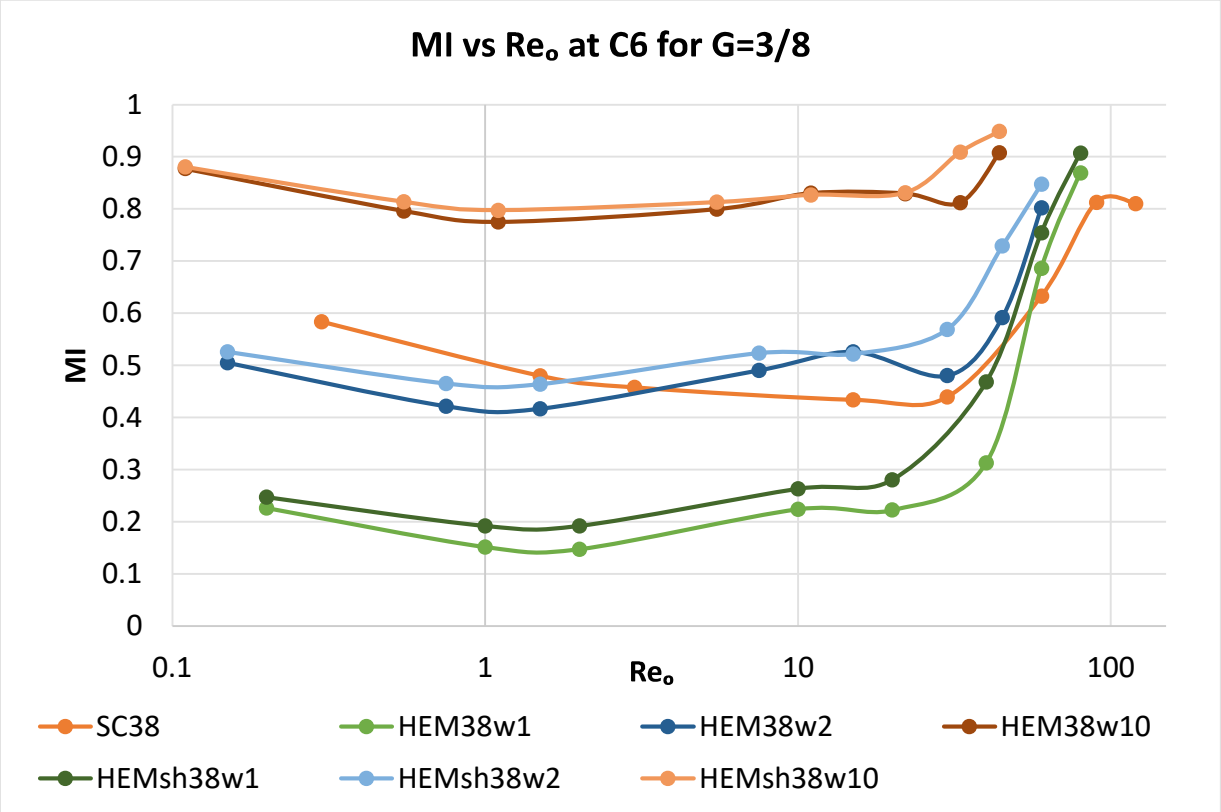

Figure 47: Details of G=3/8, C6 MI

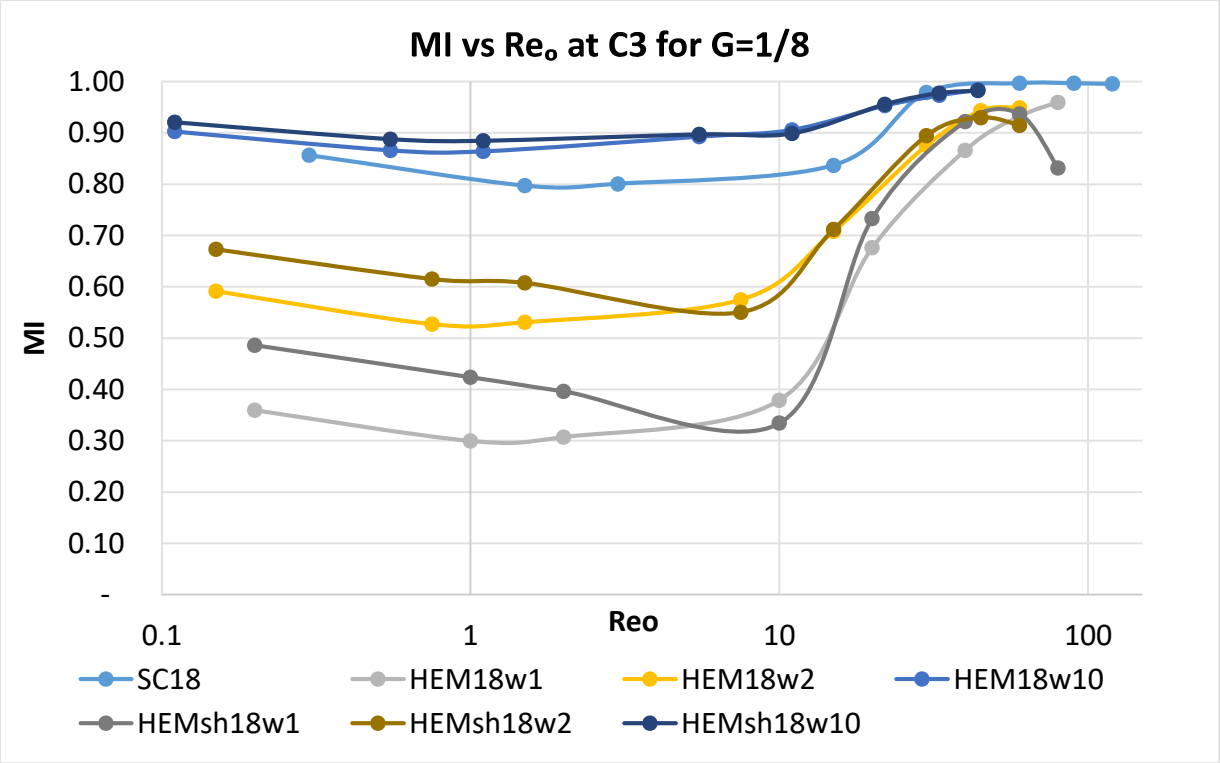

Figure 48: Details of G=1/8, C3 MI

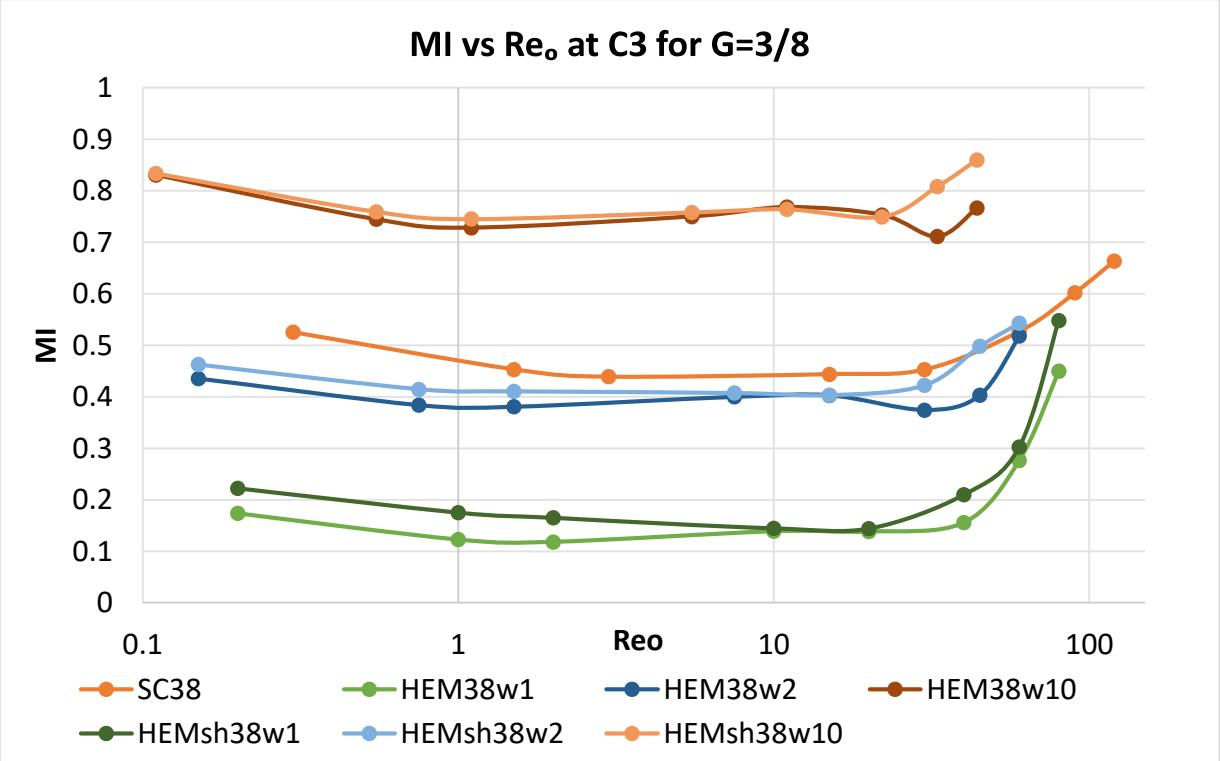

Figure 49: Details of G=3/8, C3 MI

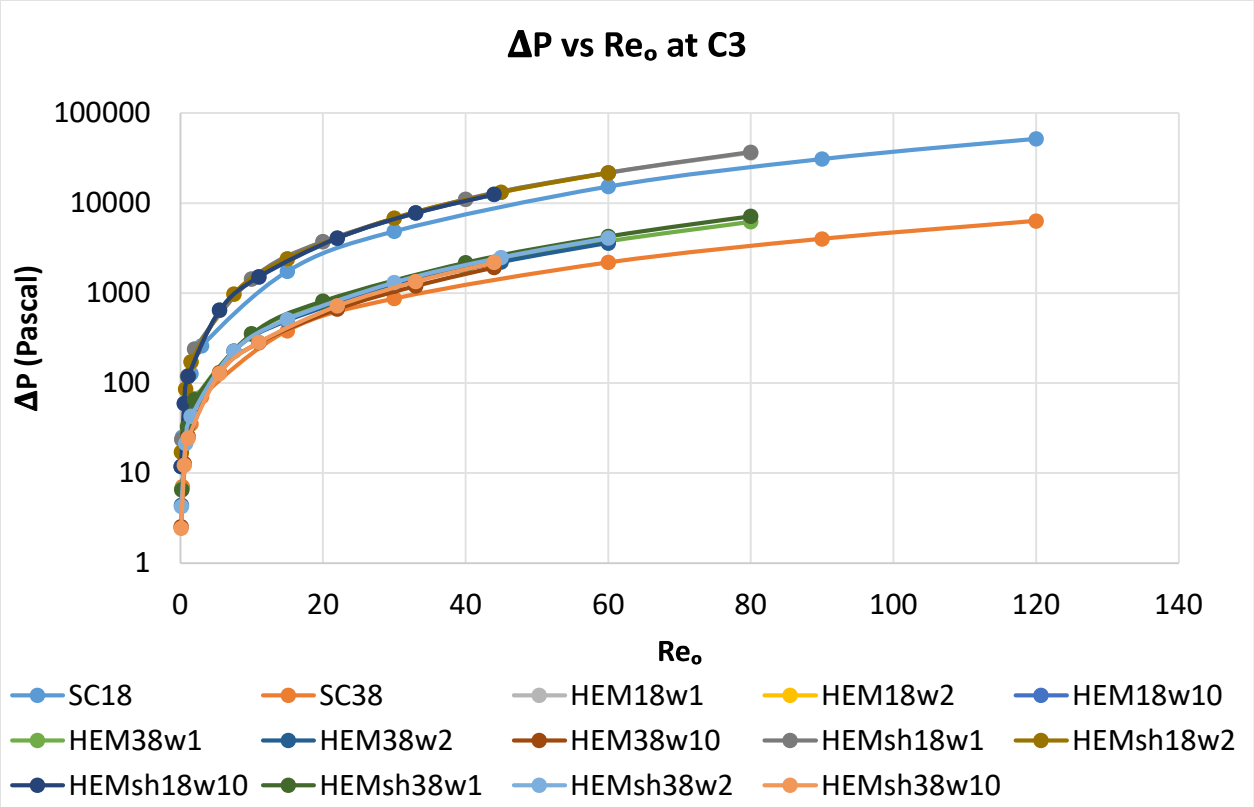

Figure 50: Details of ΔP at C3

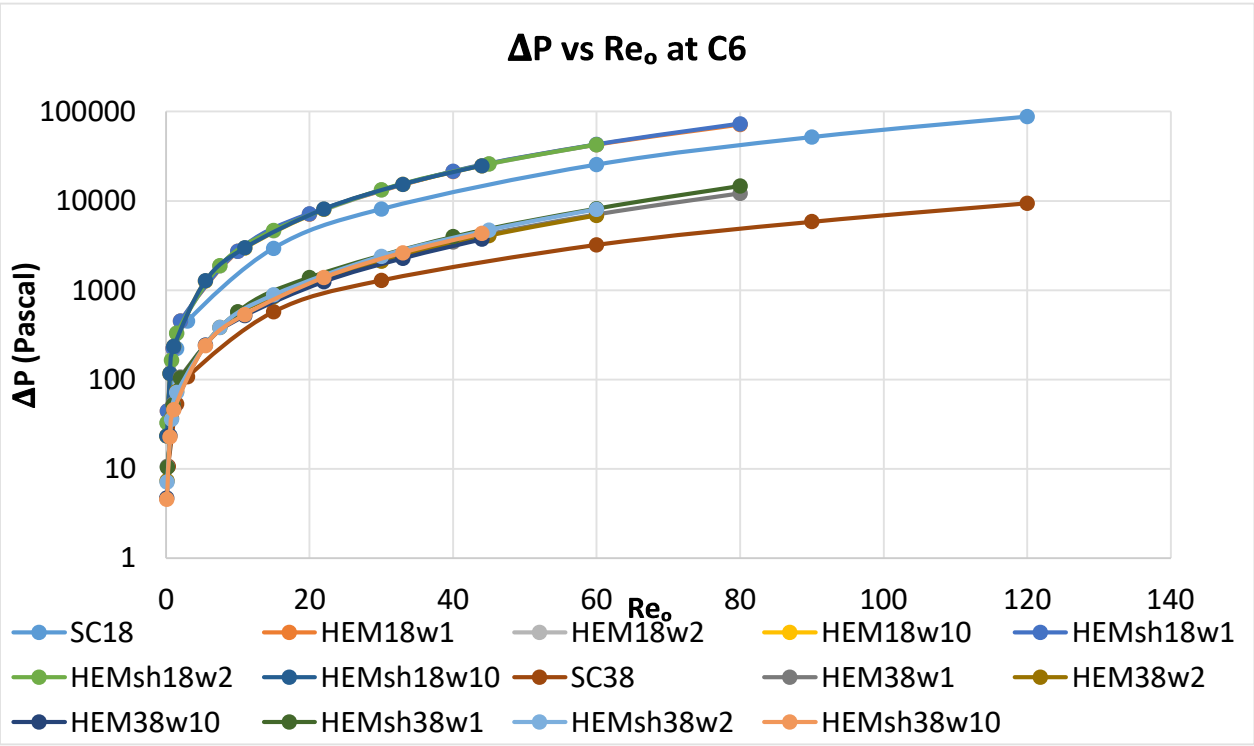

Figure 51: Details of ΔP at C6

Appendix III: Example Determination of *MI* and $\dot{s}'''$ for an Arbitrary Case

Given a tee shaped micromixer with $D_h=10\mu m$, combining fluids with similar properties to water at 300 k, where the design constraints limit the flow weight difference to $w_f = 5.6$, how would the *MI* and $\dot{s}'''$ be effected by the Reynolds number?

$$MI * P = 1.055 * 10^{-4} * Re_o + 0.037$$

$$\mathrm{P} = \left(-14.594(\mathrm{w_f}+1)^{\frac{1}{\mathrm{w}}} + 32.412\right)^{-1} \Big| w_f = 5.6 \rightarrow 0.0835$$

$$MI = \frac{1.055 * 10^{-4} * Re_o + 0.037}{0.0835} = 1.263 * 10^{-3} Re_o + 0.44311$$

Immediately, it can be determined that the minimum mixing efficiency is around 44%.

$$\frac{(\dot{\mathrm{S}}_{\mathrm{F,nd}})}{\mathrm{SF}} = (0.052\mathrm{Re_o} + 0.338) \Big| SF = 0.001 \rightarrow (\dot{\mathrm{S}}_{\mathrm{F,nd}}) = (0.000052\mathrm{Re_o} + 0.000338)$$

$$(\dot{\mathrm{S}}_{\mathrm{D,nd}}) = (0.000026\mathrm{Re_o} + 0.000033)$$

$$\gamma_1 = Re_{out}^2$$

$$\gamma_2 = \frac{2RDT_o\rho^2 D_h^2 \Delta \mathrm{C}}{\mu^3}$$

$$\overline{\dot{S}'''_{nd}} = \frac{(\mathrm{Re_o^2}(0.000052\mathrm{Re_o} + 0.000338) + \frac{2\mathrm{RDT_o}\rho^2\mathrm{D_h^2}\Delta C}{\mu^3}(0.000026\mathrm{Re_o} + 0.000033))}{V_{@t^*}}$$

$$\overline{\dot{S}'''} = \overline{\dot{S}_{\mathrm{nd}}'''} \frac{\mu^3}{\mathrm{T_o}\rho^2\mathrm{D_h^2}}$$

The remaining substitutions are all constant to the system. Plotting the results as function of the outgoing Reynolds number.

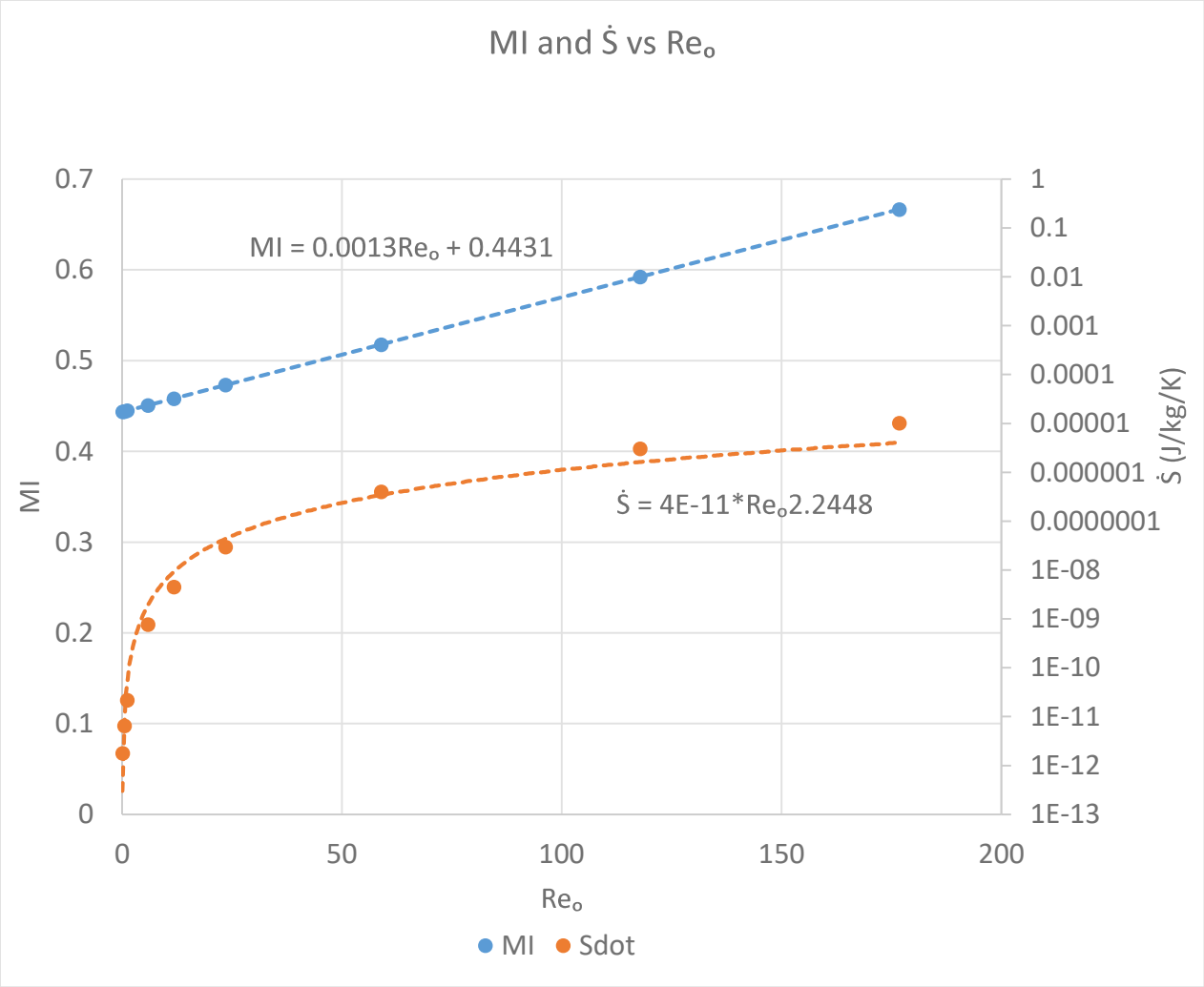

Figure 52: Results from Appendix III Example